

Chapter 1: INTRODUCTION

Proteins: Function and Primary Structure

Proteins are active molecular devices in biological systems; abundantly present in living organisms, these complex polymers play many roles in the processes that sustain life. There are proteins that maintain the structural integrity of cells, those that control gene transcription and hormone regulation, those that store and deliver vital biological molecules, those that catalyze slow processes, and those that fight off infection, among a myriad of other functions. They make up most of the bulk of every day cellular life [1].

As important as they are, proteins are composed of deceptively simple components. They are primarily composed of long amino acid strands. The general structure of an individual amino acid involves a central, chiral “ α ” carbon surrounded by a hydrogen atom, an amide nitrogen group, a carboxyl group and a side chain, usually denoted “R” unless explicitly described (**Figure 1.1**). There are twenty common amino acids in biological systems, each with a different side chain that distinguishes it from the others, and categorized as small, nucleophilic, hydrophobic, aromatic, amide, acidic or basic (**Figure 1.2**). The sequence of side chains gives a protein its primary structure [1].

In order to create the long chains that make up a protein's primary structure, amino acids undergo condensation reactions. In such a reaction, the carboxyl ($-\text{COOH}$) group of one amino acid, or peptide, becomes a carbonyl ($-\text{C}=\text{O}$) group through the loss of $-\text{OH}$, and the carbonyl carbon bonds covalently to a similarly dehydrated amide nitrogen of an adjacent amino acid, forming a dipeptide with a dispersed water molecule (**Figure 1.3**). Formation of the bond between the amino acids, referred to as a peptide bond, is a process that is repeated until a long polypeptide chain is created [2].

An important aspect of the peptide bond is its partial double bond character, which is a consequence of the ability of the carbonyl π electrons of one amino acid residue to delocalize and resonate between both the carbonyl and peptide bonds (**Figure 1.4**). This π electron delocalization creates a partially negative charge on the carbonyl oxygen and a partially positive charge on the amide nitrogen, enabling the atoms to take on a hydrogen-bond acceptor role and a hydrogen-bond donor role, respectively. This propensity for backbone solvation is important when considering protein secondary structure [2].

In addition to creating a tendency for hydrogen bonding within the polypeptide chain, the partial double bond character of the peptide bond restricts the dihedral angle (ω) between the carbonyl carbon and the amide nitrogen, so the atoms associated with the peptide bond (O, C, N and H) are confined to the same plane. This conformational limitation, along with steric hindrances created between backbone and side chain atoms, restricts the adjacent residues to a

limited range of dihedral angles. The stability of residues at different rotational orientations are illuminated by plotting the angle of rotation between the α -carbon and the amide nitrogen, phi (ϕ), against the angle of rotation between the α -carbon and the carbonyl carbon, psi (ψ), in a Ramachandran plot (**Figure 1.5** and **Figure 1.6**) [3]. The ϕ and ψ angles are the only angles of backbone rotation available to the residues in a polypeptide chain, and the Ramachandran plot reveals the combinations of both that are allowed sterically [4]. Thus, when considering the hydrogen bonding of the backbone, it is not surprising that the most stable rotational conformations of a polypeptide chain based on the Ramachandran plot correspond to those found in the two major types of secondary structure in proteins.

The polypeptide chains in a protein take on different secondary structure conformations depending on sequence, the surrounding solvent composition, pH, temperature and other energetic factors [2]. Stabilization of secondary structure in proteins is optimized if hydrophobic side chains are shielded from aqueous solvent, which in some cases can increase van der Waals interactions between them. Also, if polar side chains are exposed, the chances of their interaction with the solvent increases. The *native state* of a protein is the overall conformation it takes on in order to function properly in its biological environment. In nearly all known cases, the native state of a protein involves some folding, rather than the adoption of a completely freeform random coil, in order to optimize thermodynamic stability [3].

The two standard secondary structures common in proteins are α -helix and β -sheet. In α -helices, the backbone amide group of a residue at sequence position i forms a hydrogen bond with the backbone carbonyl group of the residue at position $i + 4$, resulting in a 100° rotation of one residue to the next in the sequence (**Figure 1.7**). Side chains of the polypeptide are directed laterally outward from the helical axis, and due to the steric favorability of peptide bonds to display *trans* orientation over *cis*, nearly all helices in proteins are right-handed [2]. The β -sheet is less common and is characterized by separate polypeptide strands (or sections distant in the sequence) lined up adjacent to one another, with backbone amide and carbonyl groups oriented in one plane of space. These amide and carbonyl groups in consecutive residues point in opposite directions in a β -sheet, and the side chains of adjacent residues point laterally either above or below the backbone axis in succession. The strands in a β -sheet can be oriented in a parallel or antiparallel fashion with respect to the N- and C-terminii of each strand (**Figure 1.7**). In parallel β -sheets, the backbone of each residue forms hydrogen bonds with two residues in the adjacent strand, which are separated by a residue between them that is not involved in that particular joining (this middle residue forms cross-links with those in the next consecutive strand). In antiparallel β -sheets, two hydrogen bonds are formed between the backbone of each residue and that of a single residue in the adjacent strand. Since the polypeptide strands in β -sheets are not completely extended, the sheet is not completely flat and takes on a pleated, zig-zag shape [1].

Many proteins possess different combinations of α -helix and β -sheet secondary structure, with other structures such as β -barrels and turns included. These combinations, along with developed tertiary structures in some cases, help facilitate the formation of binding sites and other functionalized regions that give a protein its beneficial abilities [6].

Protein Misfolding and Disease

Generally, a protein's native state structure is highly conserved over time. However, an individual protein at any instance in time may gain enough kinetic energy to overcome activation barriers, which may cause it to deviate permanently from the native state. Caustic deviations from the native structure are usually detected by mechanisms in the body, which promptly take steps to get rid of the problem [5]. Exceptions to this rule of self-cleaning in the body can be damaging over time and are a benchmark of many degenerative diseases.

The body's mechanisms for cleanup of misfolded proteins can fail for a number of reasons. In cases of a genetic mutation in DNA, the primary sequence of a protein coded during transcription can deviate from that of the native state. This change in sequence can increase the probability of misfolding in the protein, leading to the interaction between areas of the protein that are normally buried within the biological environment, causing disease. The source of these diseases is well understood due to its mutational nature [6]. Other cases of protein misfolding, however, do not have an obvious genetic cause.

Protein folding in cells occurs in a rich and crowded molecular environment, with a number of different supplementary proteins assisting in the process. There are molecular chaperones, which shield the incompletely folded protein from detrimental interactions, and catalysts, which speed up the folding process. Although these helper proteins facilitate folding in a timely manner, it has been shown that a protein will eventually fold into its native state *in vitro* when exposed to physiological conditions [6]. This finding, along with the observation that sequence mutations cause misfolding for some proteins, suggests that an important factor determining the final folded state of a protein is its primary amino acid sequence [3].

When scientists force protein folding *in vitro*, they usually do so by taking an already-folded protein and exposing it to chemicals that cause it to unfold; the folding subsequently witnessed is the result of the complete polypeptide chain working its way into the native conformation [1]. The possibilities for folding mechanisms are different *in vivo*, where the folding process could occur as the nascent chain of the protein is still in the process of being synthesized by the ribosome. With the countless structural combinations that are technically available to a protein, it would take much too long to go through each one to find the “correct” conformation via a random walk. It has been postulated, therefore, that a protein finds its native state structure through the biased selection of increasingly stable structures that are available in its energy landscape [7]. During the search for the most stable native-like state, proteins may take on less stable

intermediate forms that either do not refold into any other conformational state or, worse, may be able to “seed” other incompletely folded proteins and influence them chemically to adopt a misfolded state. Usually, molecular chaperones alleviate the consequences of these misfolded proteins and help protect the neighboring incompletely folded proteins still undergoing the conformational search, but if they appear in abundance within the cell over time, these misfolded proteins may overpower the ability of chaperones to regulate them [6].

A number of diseases have been found to be associated with protein misfolding, and visible proteinaceous deposits within organs are a key characteristic in many of them. These diseases are deemed *amyloidoses*, a term that came about after it was discovered that the aggregates in the fibrils stain with the dye Congo red in a similar way to the starch amylose [8]. Aggregates within the fibrils are called *amyloids* and the fibrils themselves *amyloid fibrils*. Based on atomic force microscopy and other studies, a proposed sequence of events for fibril formation involves a protein unfolding or misfolding into an intermediate state that is able to form β -sheets between itself and another misfolded protein. This process is repeated until large, soluble oligomers are formed, which may act as a docking station to promote other proteins to unfold and associate with it, eventually creating large insoluble fibrils (**Figure 1.8**) [9].

Amyloid fibrils are strikingly similar in appearance from disease to disease. The fibrils are usually long, on the order of about 10 nm in diameter, and share the ability to stain with Congo red and exhibit a green birefringence under

polarized light. Additionally, studies with x-ray diffraction reveal that amyloid fibrils possess an extensive β -sheet structure, with parallel and antiparallel aspects, the sheets of which are stacked atop each other perpendicular to the fibril axis [5]. Because the native structures and relative sizes of proteins involved with different amyloid diseases differ extensively among one another, the mechanism by which they can all unfold to form stable β -sheets is not well understood [10].

Amino Acid Propensities In β -Sheets

Since it is generally agreed upon that one of the first steps in fibril formation is β -sheet formation by misfolded proteins, a major focus in amyloid research is understanding the factors that go into β -sheet formation and stabilization. One notion under investigation is that certain amino acid sequences exist within proteins that have a high potential to form stable β -sheets. Hydrophobic sequences in short model peptides have been shown to form β -sheets *in vitro* [10-12], so the possibility arises that segments within proteins may aggregate with those of neighboring proteins while these structures are still in a loose, folding intermediate state. Since the folding process could feasibly begin as the chain is being produced off the ribosome (**Figure 1.9**), another possibility is that specific amino acids promote the formation of temporary secondary structures during chain development [1]. These structures could be altered according to the native state as the protein sequence elongates, but they could also be stabilized by the presence of complementary structure in a

misfolded protein nearby. The propensity for certain amino acids to encourage β -sheet formation in nascent chains may serve as a seeding mechanism for the growth of large populations of misfolded proteins over time.

While the frequency at which certain amino acid sequences appear as β -sheets is based on their physical structures, such as aromatic sequences that can facilitate π - π stacking as β -sheets [13, 14], the tendency for specific amino acids to promote certain secondary structures is vague [13]. A useful way we can discover whether certain residues are more likely to be present in β -sheets is to look through the Protein Data Bank (PDB). The data bank consists of structures of proteins that are characterized by NMR or x-ray diffraction studies. While it is still incomplete, the PDB has over 56,000 protein structures that have been determined so far, and it can be a powerful tool in the search for unexpected secondary structure partiality.

Recent reports based on a statistical PDB search show a high propensity for asparagine to be involved in parallel beta sheet structures [15]. Asparagine's polar side chain is physically capable of forming a hydrogen bond between itself and that of another asparagine side chain; this second asparagine could be present in an identical strand running parallel to it in a β -sheet, for example. The propensity was therefore reasonable until a search for glutamine preference in β -sheet orientation came up null [15]. Glutamine differs from asparagine by only one alkyl ($-\text{CH}_2$) group, causing it to extend slightly longer from the α -carbon yet

retain its hydrogen-bonding abilities (**Figure 1.10**), but its presence in β -sheets was unbiased between parallel and antiparallel orientations nonetheless.

Asparagine's statistically significant structural presence may be a consequence of the incomplete nature of the databank. It is apparent, however, that we do not yet understand the plasticity of β -sheet folding and the effects such small differences in amino acid structure may actually have during the process. Understanding why asparagine and glutamine apparently differ in their abundance within parallel β -sheets becomes an important subtlety that is examined in this thesis.

A β ₁₆₋₂₂

The peptide sequence we work with in this study is a part of the amyloid- β polypeptide (abbreviated A β), made up of between 40 and 42 residues, that is one of the main components of Alzheimer's disease and some forms of Lewy body dementia (**Figure 1.11**) [16]. The full-length A β peptides are helical in the native state but are present as one-turn β -strands that form in-register, parallel β -sheet amyloid fibrils when misfolded [17, 18]. These fibrils are present as spherical "senile plaques" in the cerebral cortexes of patients with advanced Alzheimer's disease and are thought to be the result of the disease's pathogenic benchmarks (**Figure 1.12**) [16]. Our research focuses on peptides of the sequence KLVFFAE, located in the middle of the A β polypeptide; we refer to this segment as the A β ₁₆₋₂₂ peptide. The sequence contains mainly hydrophobic residues, with a

positively charged lysine and a negatively charged glutamic acid at each terminus under neutral pH. A β_{16-22} is known to form amyloid fibrils in isolation in solid-state NMR studies (**Figure 1.13**), and particularly, these solid amyloid fibrils take on an in-register, antiparallel β -sheet conformation [19]. Recent infrared studies have also shown that A β_{16-22} adopts this antiparallel β -sheet conformation in solution at neutral pH, and that the conformation is stable to temperatures of up to 75°C [20]. At the time of this report, it is one of the shortest known amyloidogenic sequences [20].

Project Aims

The strong antiparallel β -sheet characteristics of A β_{16-22} made it a useful peptide for our purposes in this study. We set out to provide experimental evidence of whether or not asparagine's frequency in parallel β -sheets over glutamine was a tangible physical phenomenon. We took advantage of the A β_{16-22} peptide's stable antiparallel β -sheet characteristics by comparing the effects the two amino acids had on the stability or orientation of these β -sheets. Mutating the A β_{16-22} peptide at single positions with either asparagine or glutamine, we can monitor these changes using both spectroscopic and computational techniques.

Instrumentation to Determine Secondary Structure: Fourier Transform Infrared Spectroscopy

The *in vitro* portion of our work with A β ₁₆₋₂₂ involves the use of Fourier Transform Infrared Spectroscopy (FTIR), which is a type of spectroscopy that measures the vibrational excitation frequencies of various parts of a molecule and helps us determine its secondary structure.

Vibration is an intrinsic property of molecules. Because of the discrete nature of available vibrational energy states, a notion described by quantum mechanics, molecules can only absorb energy at the frequencies of vibration they themselves possess. When they absorb the energy, the molecules undergo a transition to the next allowed vibrational state. The molecule can only be excited to the next highest vibrational state, no matter the intensity of incident energy [21].

Molecules with no dipole moment will not absorb IR light. In molecules with a dipole moment, due to a polarity of electron density between atoms, the oscillation of the bond length during vibration will change the dipole moment as the atoms oscillate farther apart and closer together. Since light is in part an oscillating electric field, the molecule will only absorb IR light if it has a dipole oscillation frequency that coincides with the light's electric field oscillation frequency. With no dipole moment, the molecule cannot absorb the oscillating light [22].

The quantized nature of vibrations and the selection rule for dipoles has proven to be very convenient in the field of spectroscopy. Scientists have

developed a technique called Fourier Transform Infrared Spectroscopy (FTIR) that takes advantage of the ability of different components of a molecule to absorb energy at different frequencies in the infrared spectrum. During an FTIR experiment, a sample is exposed to a given span of the infrared region of the electromagnetic spectrum at once, and the sample absorbs the corresponding frequencies that match their vibrational frequencies. The resultant absorption data is subjected to Fourier transform, a mathematical technique that converts the data into a single spectrum with peaks at various frequencies that reflect IR absorption by the sample at those frequencies. In the case of peptides, researchers can look at the FTIR vibrational spectrum of the peptide backbone atoms to determine their orientations and interactions in space. The stretching vibrations between atoms are referred to as modes, and the resulting peaks seen in an FTIR spectrum are bands [22].

Polypeptides produce a number of bands in FTIR spectra that depict different vibrational modes of the peptide backbone. Of these, the amide I band is the most commonly used to analyze secondary structure. The amide I band results mainly from the carbonyl stretching vibration in the peptide backbone, with small contributions from out-of-phase N–H stretching. The modes for the amide I band occur at frequencies between 1600 cm^{-1} and 1700 cm^{-1} and are sensitive to hydrogen bonding and transition dipole coupling between atoms in the peptide. Since these two features of the backbone carbonyl group vary depending on secondary structure in a peptide sample, the amide I band occurs at different

frequencies in the FTIR spectrum that correlate with particular secondary structures (**Figure 1.14**). β -sheets give rise to two amide I band components that are more or less resolved depending on the orientation of strands in the sheet; antiparallel β -sheets create a sharp peak at $\sim 1620\text{ cm}^{-1}$ and a smaller peak at $\sim 1690\text{ cm}^{-1}$, while parallel β -sheets create a sharp peak at $\sim 1620\text{ cm}^{-1}$ with a smaller peak at $\sim 1636\text{ cm}^{-1}$ (**Figure 1.15**) [22].

The amide I band is very close in the infrared spectrum to the band resulting from O-H scissoring motion of liquid water, so the presence of water in the sample can cause poor resolution of the amide I band. Using deuterium-based solvent helps avoid this problem. With a larger reduced mass from the neutron in deuterium, the frequency of vibration of the deuterated water molecule shifts downfield, away from the amide I band (denoted amide I' after exchange). The amide I mode is also nearby the amide II band, created mainly by N-H stretching, although these bands are not as severely overlapping as the amide I and water bands. $^1\text{H}/\text{D}$ exchange that occurs on the amide groups in a peptide sample upon deuterium-based solvation causes the amide II mode to lower in frequency by $\sim 100\text{ cm}^{-1}$ (now called the amide II' band), providing a larger separation between it and the amide I band (now called the amide I' band) [22].

The difference in band splitting between antiparallel and parallel β -sheets allows us to pinpoint the specific orientation of strands within β -sheets in a sample, which is extremely useful in determining the effects of asparagine and glutamine substitutions in the $\text{A}\beta_{16-22}$ peptide. Also, unlike NMR solid-state

techniques, samples in FTIR can be analyzed under turbid conditions in a liquid state because only global secondary structure, not site-specific structure, is measured [23]. This caveat in FTIR highlights the benefits of studying a small amyloidogenic peptide like A β_{16-22} .

Approximating β -Sheet Stability: Molecular Dynamics Simulations

It would be advantageous in our study to be able to see the specific atomic interactions that determine the differences in stability between mutated A β_{16-22} peptides when they are arranged as parallel β -sheets. Although it is impossible experimentally to observe the peptides with such precision, computational chemistry may allow us to predict this atomic behavior through molecular dynamics (MD) simulations. Advancements in computer technology in recent years have allowed researchers to model the behavior of protein systems over long periods of time using statistical functions that approximate molecular interactions with increasing accuracy. The dynamic and thermodynamic elements of internal motion in proteins are both important aspects to consider in these functions. The dynamics part of MD simulations focuses on the displacement of different parts of the system from the average over time, while the thermodynamics addresses the equilibrium of the system at any given point, information that subsequently influences the dynamics trajectory [24].

At a given time, a polypeptide exhibits a wide range of motions that contribute to its overall structure. The smallest effective units of a molecule that

are used to promote energetically significant changes in molecular dynamics simulations are those whose atoms move as a group due to covalent bonding. Examples include the aromatic portions of side chains, the isopropyl groups in the side chains of valine and isoleucine, and the peptide bond atoms in the polypeptide backbone. These units display relatively small internal motion due to the large energy cost associated with deforming bond lengths, bond angles or dihedral angles about multiple bonds, so they tend not to deviate from their nearly rigid forms [23]. Relevant motions that do contribute to peptide MD simulations, therefore, involve the relative displacements caused by torsion about the single bonds that link the rigid units together, such as rotations about the phi and psi dihedral angles and those within single-bonded side chain segments.

The dynamic trajectory in MD simulations is conducted as a function of time, and different motions require different amounts of time to occur. Most rigid units in a protein are encaged by other atoms in the protein or by those in the surrounding solvent; at short time scales, on the order of 10^{-12} seconds, these units can take on rattling motions in their “cages” that displace them a short distance (less than 0.2 Å). While small in scale over a short amount of time, and thus not a huge promoter of drastic structural changes at such time scales, these local motions can be substantial over longer time intervals if each successive fluctuation pushes the system toward a lower internal energy. The changes in larger regions of the protein structure as a result of these small fluctuations, such as β -sheet twisting, can be seen over time scales ranging from nanoseconds to

seconds. Dramatic structural changes within a protein during a simulation, such as transitions from folded to unfolded states, are usually seen within second to 10^4 second timescales [24].

In addition to the locomotive possibilities a protein has due to covalent bonding, there are several noncovalent interactions within a protein that influence its stability, and simulations must take them into account in order to provide realistic trajectories. In the case of the $A\beta_{16-22}$ mutants of this study, hydrogen bonding between strands in the β -sheet structure helps constrict the motion of atoms, while van der Waals' attractions between regions with large electron clouds play a role in keeping certain regions like interstrand phenylalanines nearby in β -sheets. Electrostatic interactions play perhaps the largest role besides covalent bonding in the motion of atoms in the peptides; for instance, oppositely charged residues within strands can promote or discourage interstrand attraction. Finally, simulations work under specific environmental conditions such as pH, solvent saturation and temperature, specifications that are an important factor in determining the energetic stability of the peptide being simulated.

Molecular dynamics simulations work in a "stop-go" fashion, allowing dynamics to occur for a short time before pausing, calculating the new internal energy within the system, and restarting the movement, which changes in response to the new energy [24]. In order to facilitate realistic trajectories, the starting structure in a simulation must be equilibrated in energy, according to the statistical abilities of the program, so that the system in the specified

conformation has the lowest possible starting energy before the start of trajectories.

Increasing the temperature of the system can provide enough kinetic energy to overcome the activation barriers associated with the deep well in the energy landscape. Once through this activation barrier, the system may find itself on a path toward a deeper well whose conformation offers even lower internal energy during the simulation, where it will remain centered unless the environmental conditions are changed favorably. Temperature modification is useful when comparing the stabilities of two systems that differ in only one place; the different energy wells into which the two systems fall thermodynamically can elucidate specific atomic interactions the alterations promote. In this vein, we aim to utilize temperature controlled MD simulations to probe the specific effects of asparagine and glutamine substitutions on the stability of A β_{16-22} parallel β -sheet dimers. With the experimental data from FTIR on these same peptides, we hope to be able to obtain a better understanding of the differences in thermodynamic properties between asparagine and glutamine in A β_{16-22} β -sheet formation.

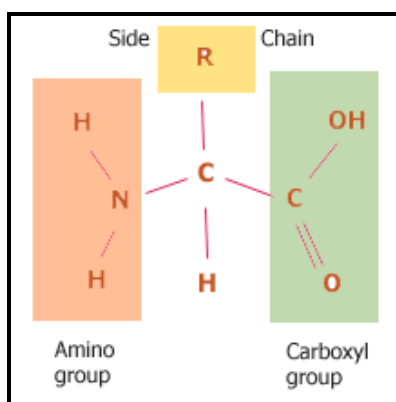


Figure 1.1 – The structure of a generic amino acid. The central α -carbon is flanked by a hydrogen atom, an amino group (red), a carboxyl group (green) and a side chain (yellow). The structure of the side chain is the distinguishing feature among different amino acids. [25]

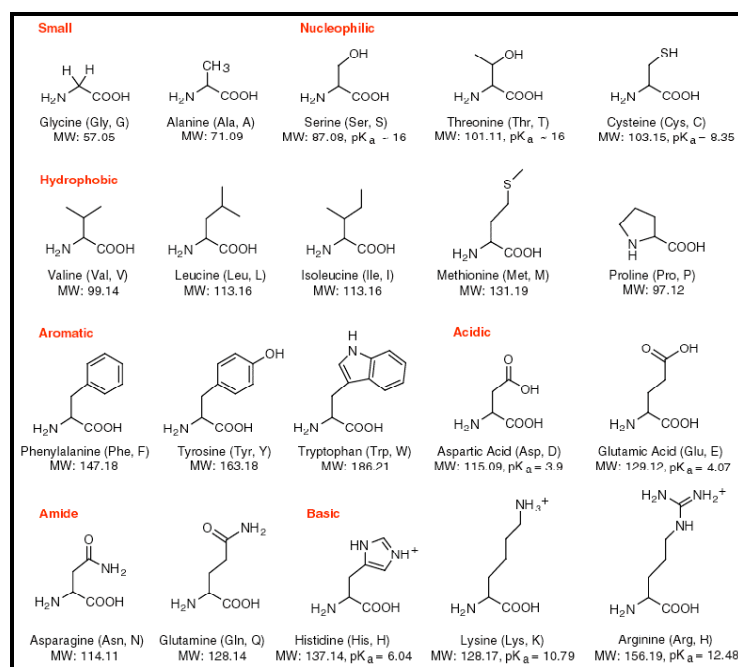


Figure 1.2 – The twenty most common natural amino acids. Each amino acid is categorized based on the chemical properties of its side chain. [26]

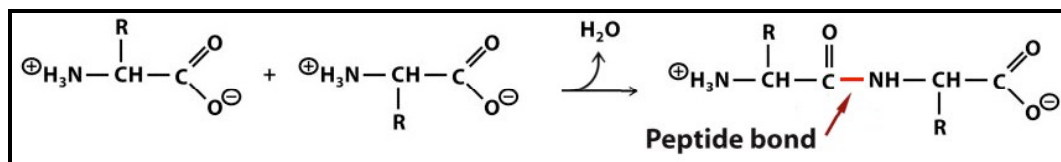


Figure 1.3 – Formation of the peptide bond. A dehydration reaction occurs between the amino group of one amino acid and the carboxyl group of another amino acid, dispersing a water molecule and forming a peptide bond, shown in red. [27]

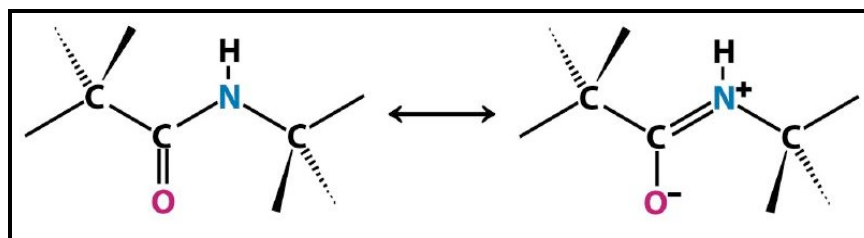


Figure 1.4 – The resonance structures of a peptide bond. Electrons in the π orbital of the carbonyl double bond are able to delocalize from the carbonyl bond into the peptide bond, creating a partial charge on both the oxygen and nitrogen atoms. This resonance results in the partial double bond character in the peptide bond. [28]

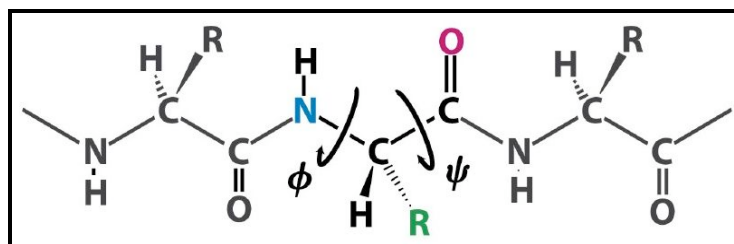


Figure 1.5 – The phi (ϕ) and psi (ψ) dihedral angles of rotation in the backbone of a polypeptide. These angles determine the torsion characteristics of the peptide backbone that are important in secondary structure conformation. [29]

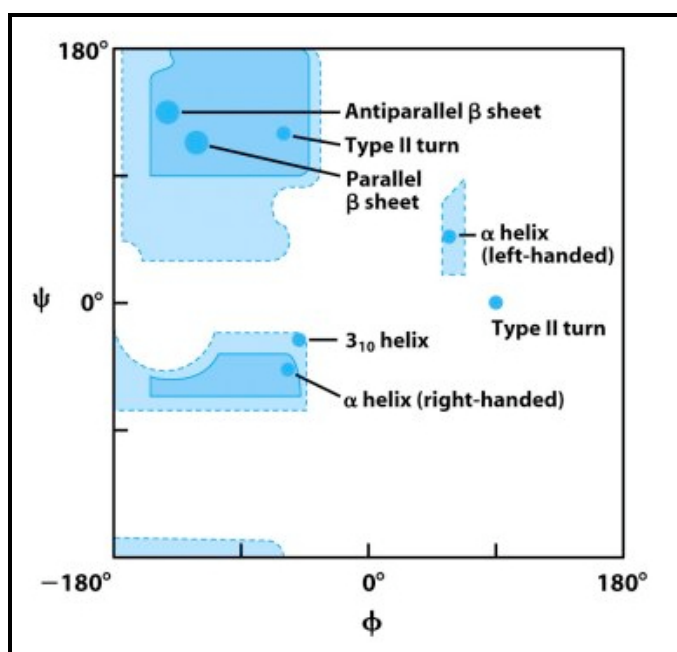


Figure 1.6 – The Ramachandran plot. This plot describes the possible values of the phi and psi dihedral angles that result in favorable sterics within proteins. The larger, more favorable regions in the plot correspond to dihedral angles found in the β -sheet and α -helix secondary structures commonly found in proteins. [30]

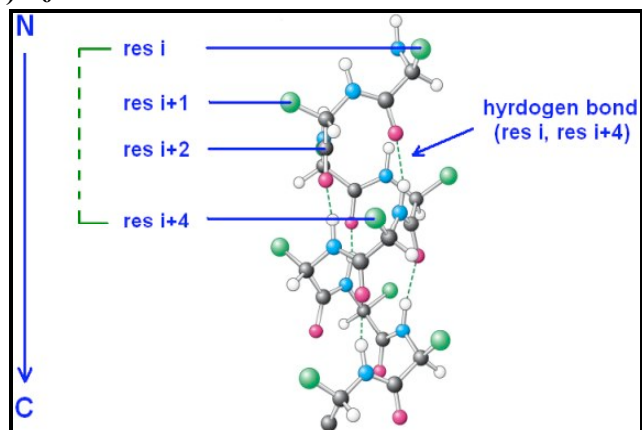
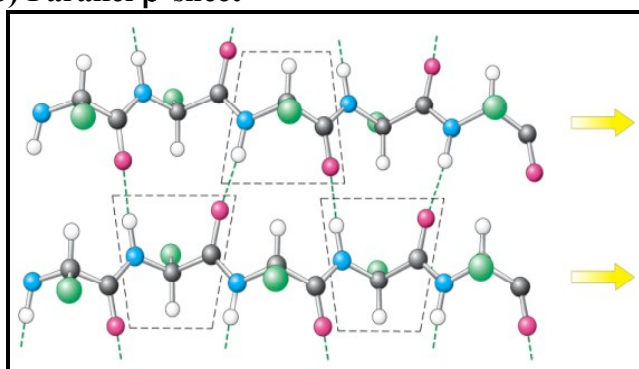
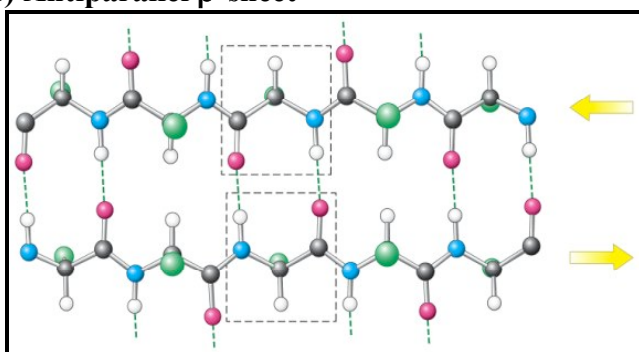
a) 3_6 α -helixb) Parallel β -sheetc) Antiparallel β -sheet

Figure 1.7 – Common secondary structures in proteins. The 3_6 α -helix (a), parallel β -sheet (b) and antiparallel β -sheet (c) orientations are shown. Example residues in β -sheets are boxed (---) for clarity. Atoms in the structures are represented with spheres: carbon is black, nitrogen is blue, oxygen is red, hydrogen is white, and the R groups of each residue are reduced to a single green sphere. Hydrogen bonds are depicted by green dashed lines. [31]

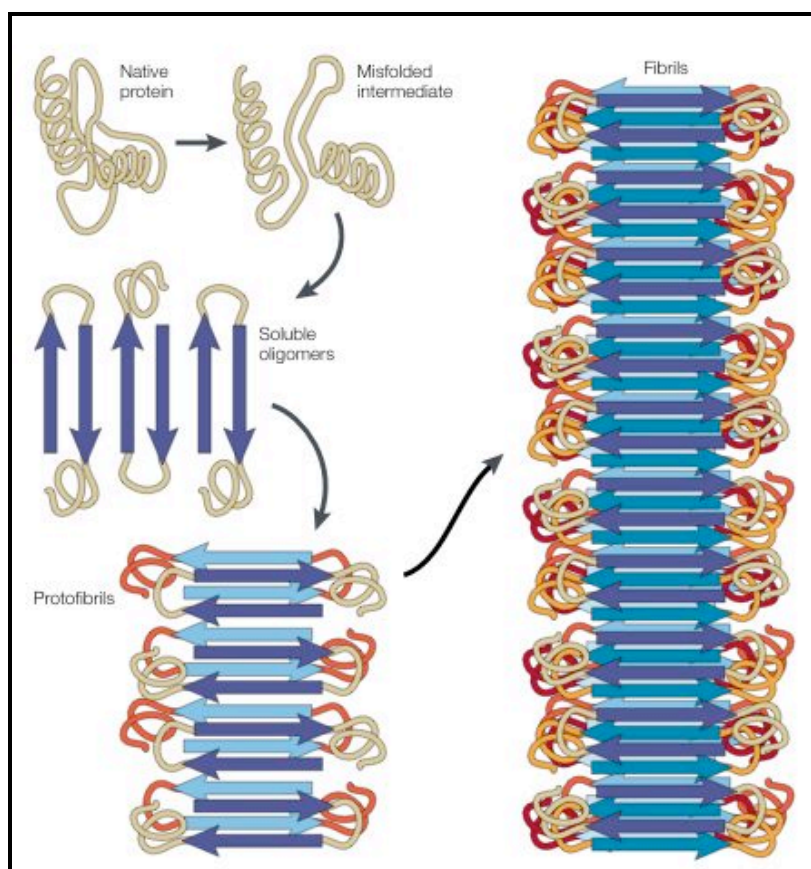


Figure 1.8 – Amyloid fibril formation. The proposed mechanism involves first the native state protein misfolding, which forms soluble β -sheet oligomers that promote unfolding of other proteins to form thickening protofibrils, which eventually grow into large, insoluble fibrils. [32]

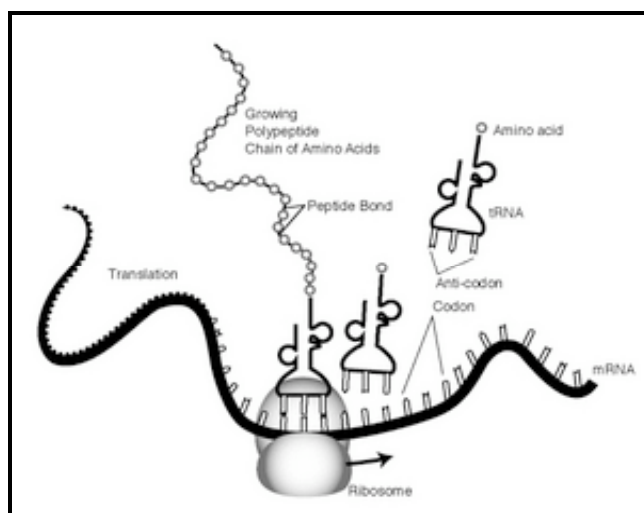


Figure 1.9 – The formation of nascent peptide chains. The ribosome serves as a docking site for charged transfer RNA molecules to bind to DNA, where they release their accompanying amino acid to be incorporated into the nascent peptide chain. [33]

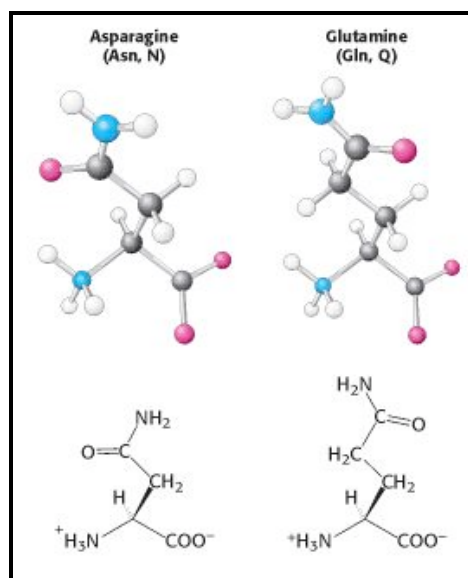


Figure 1.10 – Structures of the asparagine and glutamine amino acids. These amino acids make up the amide category of the 20 most common natural amino acids. Side chains on both amino acids end with a carboxamide functional group, but the side chain of asparagine is one methylene group shorter than that of glutamine. [34]

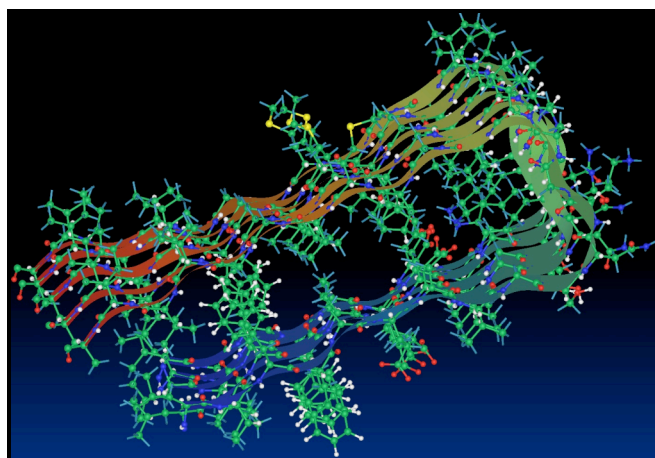


Figure 1.11 – The Structure of the Amyloid- β polypeptide as seen in the Protein Data Bank. The peptide takes on an extended β -sheet formation with a characteristic β -turn when incorporated into amyloid fibrils. [35]

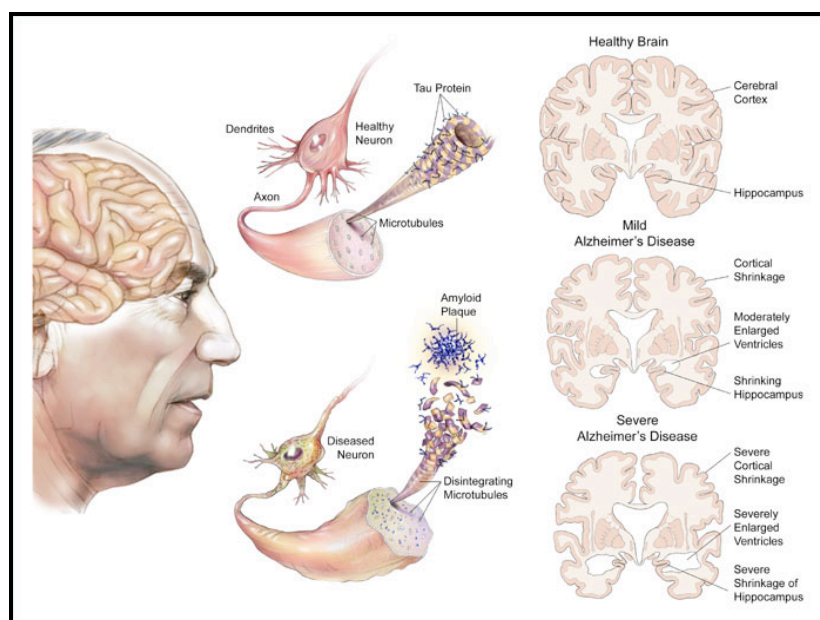


Figure 1.12 – Alzheimer's Disease. A main constituent of the disease is the formation of amyloid- β plaques in neuronal tissue, seen in the center of the image. [36]

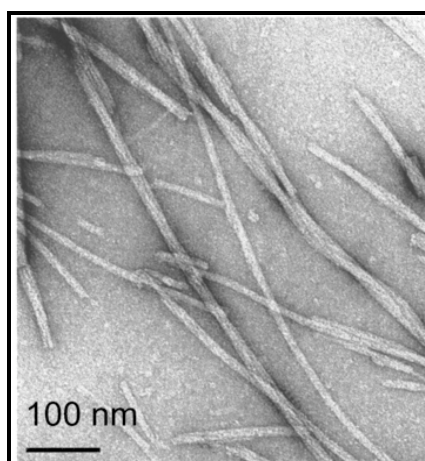


Figure 1.13 – $A\beta_{16-22}$ amyloid fibrils as imaged by transmission electron microscopy. The fibrils were negatively stained with uranyl acetate to allow for better visualization. [19]

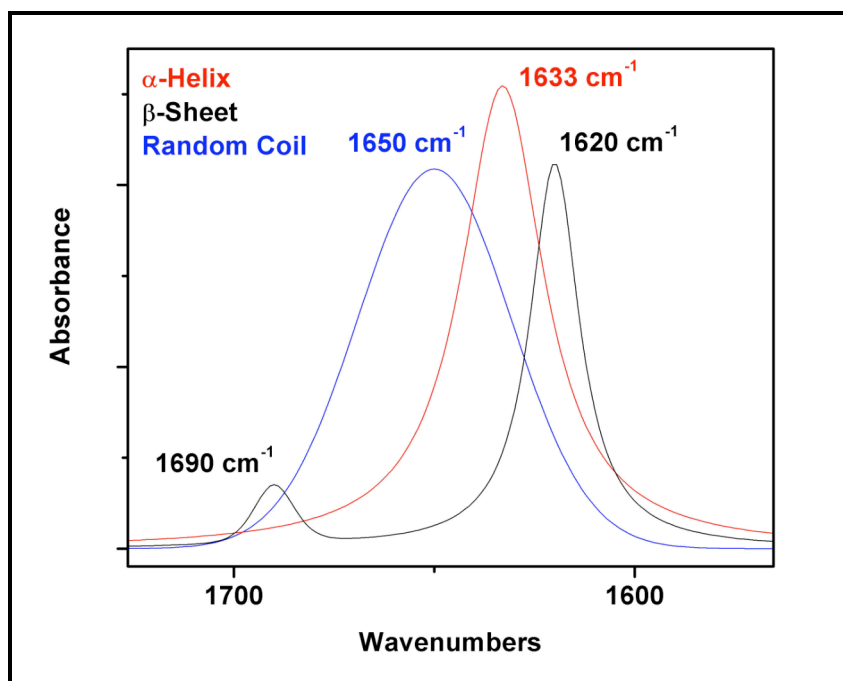


Figure 1.14 – Secondary structure sensitivity of the protein amide I' band in Fourier transform infrared spectroscopy. The amide I' band occurs as a broad peak at $\sim 1650\text{ cm}^{-1}$ when the protein has a random coil conformation (blue), as a peak at $\sim 1633\text{ cm}^{-1}$ for α -helical structures (red), and as two peaks, one at $\sim 1690 - 1636\text{ cm}^{-1}$ and the other at $\sim 1620\text{ cm}^{-1}$, for β -sheet conformations (black).

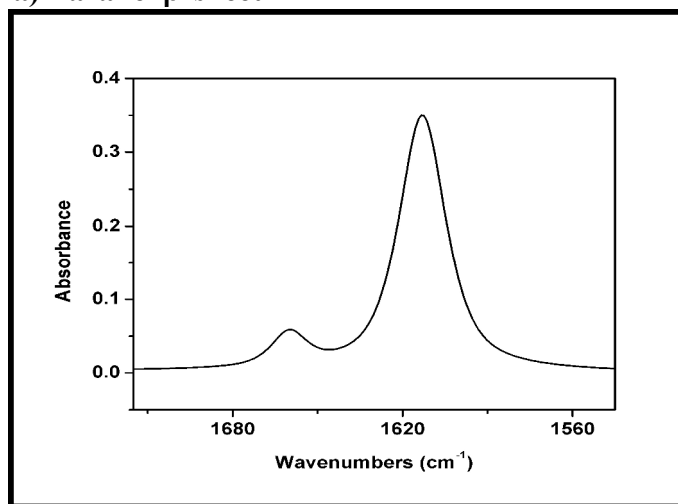
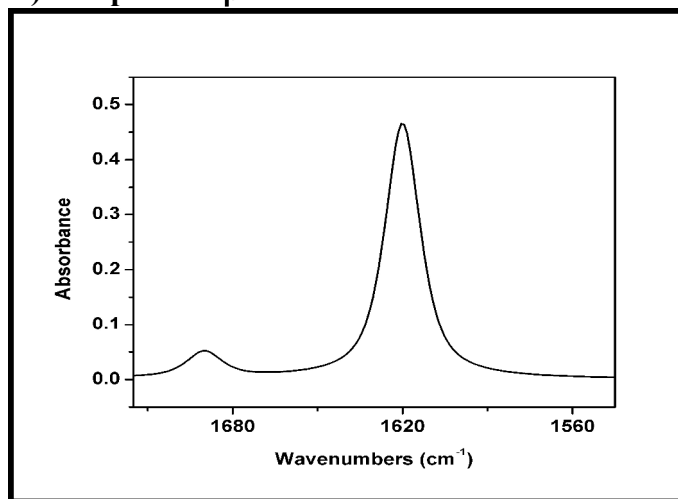
a) Parallel β -sheet**b) Antiparallel β -sheet**

Figure 1.15 – Amide I' bands depicting different β -sheet orientations in Fourier transform infrared spectroscopy. Resolution of the two β -sheet amide I' bands is reduced in parallel β -sheets (**a**), while two characteristic peaks, one at ~ 1620 cm⁻¹ and the other at ~ 1690 cm⁻¹, are present for antiparallel β -sheets (**b**).

Chapter 2: MATERIALS AND METHODS

Solid Phase Peptide Synthesis

SPPS Background

Peptides were synthesized using a CEM LibertyTM microwave accelerated peptide synthesizer. Peptides are added sequentially in a C-to-N-terminal fashion onto an insoluble polymer resin support (**Figure 2.1**).

Amino acids are provided in a protected form to ensure that unintended polymerization does not occur during peptide synthesis. The Fmoc (9-fluorenylmethyl carbamate) protecting group is attached to the α -amino group on each amino acid provided, and is also attached to any side chains that contain reactive groups. To start the synthesis, the C-terminus protected amino acid is added to the insoluble resin via the reaction of the carbonyl group of the amino acid with a reactive group on the resin. The Fmoc protective group is then removed from the amino acid with a mild organic base (20% piperidine in N,N-dimethyl formamide (DMF) in this case), leaving it open to polymerization by other amino acids.

At this point, the synthesizer performs a DMF wash to remove excess piperidine in the system, and the second amino acid in the desired sequence is introduced in its protected form. The protected amino acid undergoes activation at

the carbonyl group by tetramethyluronium hexafluorophosphate (HATU) in DMF and diisopropylamine (DIEA) [37]. This activation is provided in order to speed up the polymerization of the new amino acid to the first amino acid in the desired sequence by making the oxygen on the carboxylate end of the amino acid a better leaving group and quickening the coupling of the two amino acids. The Fmoc protecting group on the second amino acid is removed with the mildly basic piperidine deblocking reagent, and the linking process is repeated until the desired peptide sequence is synthesized. The entire sequence building process is monitored using Fmoc absorbance at 365 nanometers. The resin, with amino acids attached, must be washed in between couplings to ensure that any excess reactants from the previous coupling are removed from the environment.

After synthesis of the desired peptide is completed, the sample undergoes a final deprotection step and cleavage from the resin. To do this, a solution of trifluoroacetic acid (TFA), triisopropylsilane (TIPS) and distilled water is introduced to act as a mild acid to remove side chain protecting groups and peptide-linker bonds. TIPS removes these released protecting groups from solution [37]. The final crude synthesized peptide is precipitated in cold ether, to be purified using High Performance Liquid Chromatography.

SPPS Protocol

Refer to **Table 3.1** for a list of the peptide sequences synthesized in this study. The resin used in the synthesis consisted of a polyethylene glycol grafted polystyrene support (PEG-PS) with a 5-(4-Fmoc-aminomethyl-3,5-

dimethoxyphenoxy) valeric acid (PAL) linker; this resin was provided in certain abundances depending on the amount of peptide desired at the end of synthesis. Fmoc-protected amino acids were provided in a four times excess for the 0.100 mM scale reactions.

Cleavage from the resin was conducted using the TFA and TIPS scavenger solution, and the cleaved solution was then mixed with 70 milliliters of cold *tert*-butyl ether to be left to precipitate overnight at -20°C . After precipitation, the suspension was centrifuged at 10°C at a speed of 8000 rotations per minute for 15 minutes. The resulting peptide pellet was resuspended in 10 milliliters of distilled water and 2 milliliters of acetonitrile to assist in dissolving, and finally freeze-dried with liquid nitrogen and lyophilized as preparation for purification.

Peptide Purification: High Performance Liquid Chromatography

HPLC Background

A number of impurities exist in the crude sample after synthesis; incomplete segments of peptide could be present, as well as extraneous protecting groups and resin particles. High Performance Liquid Chromatography (HPLC) is a method used to remove these impurities from the peptide after synthesis (**Figure 2.2**). HPLC takes advantage of the non-covalent interactions that promote attraction or repulsion between different substances depending on their molecular properties. The system involves the manipulation of a mobile phase to create a

gradient elution of different components of the sample from the stationary phase, or column. The mobile phase in HPLC refers to the solvent being continuously applied to the column and acts as a carrier for the sample solution upon injection. The stationary phase refers to the solid support contained within the column over which the mobile phase continuously flows. Reversed-phase HPLC is utilized in this study and operates on the basis of hydrophobicity and hydrophilicity [1]. In reversed-phase HPLC, the column consists of silica-based packings with *n*-alkyl chains covalently bound to them. Increasing the number of alkyl chains in the column matrix increases the hydrophobicity of the column, and the tendency of the column to retain hydrophobic molecules increases.

The following sequence of events occurs in reversed-phase HPLC of a peptide. A solution containing the crude peptide sample is injected into the mobile phase through the injector port. The mobile phase usually contains trifluoroacetic acid (TFA), a negatively charged molecule at neutral pH that associates with the peptide and allows for better adherence and detachment of the peptides to and from the column. The exact mechanism by which TFA promotes better interaction between peptides and the stationary phase is not well elucidated, but using the substance in HPLC purification of peptides has become standard practice nonetheless. As a sample solution flows through the column with the mobile phase, the components of that solution migrate and interact with the column according to their molecular affinity to it. Components that have stronger

attractive interactions with the mobile phase than with the stationary phase will elute from the column faster, and vice versa.

The properties of the mobile phase can be altered in order to manipulate the interactions of the sample and the stationary phase. In gradient elution, the sample is initially injected while a less hydrophobic mobile phase, like water, is being applied to the system. The hydrophobic strength of the mobile phase is increased in a linear fashion throughout the run by raising the amount of organic, hydrophobic solvent present among the hydrophilic solvent. A common organic solvent used in peptide purification is acetonitrile. The percentage of organic solvent in the mobile phase is referred to as %B, and the increase in %B subsequently results in elution of retained components from the column at different points in time based on their degree of hydrophobicity.

A UV/Vis spectrophotometer is located at the end of the HPLC device and determines the absorbance of light by the mobile phase and its eluted contents at selected wavelengths as they leave the column. The molecule of interest in the purification process absorbs light at a specific wavelength and, in the case of this study, with a marked intensity, so its elution from the column can be monitored. An automated rack with rows of test tubes continuously collects small successive amounts of the mobile phase after it is analyzed spectrophotometrically. This fraction collection system allows for the researcher to gather the portion of the mobile phase that corresponds to the peak of interest in the UV/Vis data, concluding the purification process.

HPLC Protocol

To purify peptides after synthesis in this study, a Pharmacia AKTA™ basic 10/100 HPLC instrument was utilized with a Vydac C18 column. The crude peptide was dissolved in filtered distilled water with 0.1% TFA to create a 5 mg/mL solution. Filtered HPLC grade acetonitrile with 0.085% TFA was then added to the solution to allow the peptide to further dissolve; the maximum ratio of peptide to acetonitrile was 8 mg/mL. To assist in dissolving, the solution was vortexed and sonicated for five to ten minutes.

Approximately 4 mL of the prepared sample was loaded into the sample column via syringe after the column was rinsed with distilled water to ensure its cleanliness. Analysis of the runs was performed on UNICORN version 3.00.10. The method settings in UNICORN allowed the amount of 0.085% TFA acetonitrile, the organic solvent in the eluting process, to increase from a concentration of 15% to 40% in 0.01% TFA water as this mobile phase flowed through the column to elute the peptide. The UNICORN program monitored wavelengths of the eluting solution at 220 nanometers and 274 nanometers, and the peptide was collected at a rate of 8 mL/minute in fraction collecting tubes when its large corresponding peak appeared in the 220 nanometer wavelength range. Immediately following the fraction collection, the purified peptide was transferred to clean falcon tubes and frozen in liquid nitrogen before being placed into the lyophilizer for drying. The frozen peptide was lyophilized for 24 hours or until completely dried.

Fourier Transform Infrared Spectroscopy

FTIR Protocol

In order for the amide I' band of the peptide to be shifted away from that of the scissoring O-H bonds in water, the purified peptides were dissolved and exchanged in 0.05M deuterium chloride in deuterium oxide solvent at a ratio of 2 mL/mg for at least six hours. This action exchanges the hydrogen atoms in the peptide with deuterium, a slightly heavier atom. With the heavier atom on the amide group of the backbone in the peptide, the amide II' mode in FTIR will appear at a lower frequency and be distinguished from the O-H mode.

Peptide exchange with acidic deuterium oxide also removes residual trifluoroacetic acid (TFA) from the sample by protonating its carboxyl group, which neutralizes it. The carbonyl group in TFA creates a sharp band in FTIR that occurs at a frequency similar to that of the amide I' band, so neutralizing TFA will help remove it from the sample. Neutralized TFA no longer associates with the peptides and is subsequently removed from the sample during lyophilization.

To examine the aggregation characteristics and thermostability of the purified A β ₁₆₋₂₂ peptide derivatives, FTIR Spectroscopy was utilized using a Bruker Vector 22 spectrophotometer. The dried peptides were dissolved in a 1 mM potassium phosphate buffer solution at pH 7.06 and at a concentration of 1.5 mg/ μ L. For each sample scanned, 60 μ L of the prepared peptide were placed

between two calcium fluoride polished discs (19 mm × 2 mm) with a 0.100 mm thick, 19 mm wide Teflon ring used as a spacer.

Temperature scans were taken for each A β ₁₆₋₂₂ peptide derivative in question, increasing in 10°C increments from 25°C to 75°C, after which the temperature was lowered back to 25°C to examine any reversibility behavior that might occur with the decrease. The temperature of the sample was controlled using a NESLAB NTE-111 circulating water bath. Between each increase in temperature was a 900 second delay to allow for the sample to adjust to the change. The settings during each run included a resolution of 4 cm⁻¹, 512 scan repetitions, which were averaged together to give a final spectrum, and a range of data was collected from 4000 cm⁻¹ to 400 cm⁻¹. To keep the samples as dry as possible during each scan, molecular sieves, 4A, beads 8-12 mesh were present in the spectrophotometer cavity, which was purged with nitrogen gas for at least 30 minutes prior to and during the scans to minimize water peaks in the spectrum.

To assist in the data processing step of FTIR analysis, scans of unpurged air, nitrogen purged air and 1 mM potassium phosphate buffer were also completed. Data was collected for each temperature using OPUS software and transferred to GRAMS/32 version 5.10 for analysis. During processing, the purged air spectrum was subtracted from each sample spectrum to convert each spectrum from transmission to absorbance. The peaks associated with the buffer were subtracted next by subtracting the buffer spectrum from each sample spectra. Finally, water vapor was eliminated from the sample spectra by subtracting the

water vapor spectrum, which was produced from the purged air and unpurged air scans. In order to examine the different temperature spectra of a peptide sample as a group, the baseline of each spectrum had to begin at the same place on the y-axis, and so the baseline of each spectrum was adjusted to allow easier visualization.

Molecular Dynamics (MD) Simulations

MD Protocol

The computational portion of the study involved building *in situ* solvated dimers of A β ₁₆₋₂₂ peptide derivatives, oriented in predetermined parallel β -sheets, and subjecting the systems to a forcefield that calculates various dynamic interactions between atoms in the system with an increase in temperature. We used the CHARMM27 forcefield in these simulations. This force field was specifically designed for protein simulations and utilizes classical mechanical functions that approximate several motions among atoms in the system as they seek accessible minimal energy states (**Figure 2.3**) [38].

The Molecular Operating Environment (M.O.E.) software was used to conduct the CHARMM27 simulations during June 2006 in the Department of Pharmacology at Robert Wood Johnson Medical School of the University of Medicine and Dentistry of New Jersey under the direction of Professor William J. Welsh.

Parallel β -sheet dimers of both the L17N and L17Q mutants of the $A\beta_{16-22}$ peptide were subjected to MD simulations, as well as of the wild-type structure, which was used as a control. The initial coordinates for structures in the simulations were obtained from the Protein Data Bank (PDB), an online database of protein structures elucidated by x-ray crystallography and NMR, operated by the Research Collaboratory for Structural Bioinformatics. At the time the simulations were run, we were not able to find a published structure of parallel $A\beta_{16-22}$ β -sheets, so instead the parallel β -sheet fibril structure of the full-length 42-residue $A\beta$ polypeptide, determined via NMR by Luhrs et al. at the Salk Insitutie for Biological Studies, was used [35]. The PDB reference code for this structure is 2BEG.

The molecular structure of a single fibril polypeptide from the 2BEG file was imported into M.O.E., where residues surrounding those in positions 16 through 22 were deleted. This created a single $A\beta_{16-22}$ strand with dihedral angles similar to those found in real $A\beta$ parallel amyloid fibril samples. The resulting peptide was acylated and amidated at the N- and C-termini, respectively, to provide peptide capping similar to that of peptides examined in the wet lab experiments. Also, the lysine and glutamic acid side chains were protonated and deprotonated in the peptide to create positive and negative charged states, respectively; the peptide was saturated in all other available regions. This modified peptide was duplicated using a selection feature in the program, and the two strands were aligned in a parallel fashion adjacent to one another in the 3-

dimensional matrix, with approximately 4.6 Å separating the amides and carbonyl groups between the backbones to facilitate hydrogen bonding. This final coordinate structure was saved and used as a template for the wild-type A β ₁₆₋₂₂ as well as for the two derivatives. Mutations in the derivatives were carried out using the sequence editor option in the program that switched the leucines at position 17 in each strand with asparagine, data which was saved for the L17N simulations, and glutamine, for the L17Q simulations. Both new amino acids possessed standard dihedral angles as delegated by M.O.E. when they were incorporated into the peptide.

Once the initial coordinates of each set of dimers were established, they were subjected to energy minimization. This process uses the selected CHARMM27 force field to calculate trajectories from the starting conformation that result in increasingly lower energies for the system until it arrives at a local minimum in the energy landscape (**Figure 2.4**). Energy minimization of the dimers in this study were conducted using an implicit Born solvent function that mimics the overall electrostatic influences an aqueous solvent would have on the peptides; this solvent effect is continuous throughout the system, and explicit water molecules were not employed during the simulations. Partial charges in the peptides were also calculated during minimization, which further influenced the trajectory. A statistical gradient of 0.000001 was set up for the minimization process for dimers in this study. The statistical gradient is a value that describes the sensitivity with which the conformational searching will occur. At this small a

gradient, subtle changes in the energy during minimization will be taken into account near the end of the process, resulting in a more accurate value for the bottom of the energy well and a minimized starting conformation for the simulation.

MD simulations were conducted following energy minimization for each of the three derivative dimer structures. Force field functions enabled during the simulations included those that calculate bond stretch, angle bend, stretch-bend, torsion, out of phase bend, van der Waals', and electrostatic interactions, while a cutoff distance for calculations between distant atoms was set to 8-10 Å. A periodic boundary was also established in the system. Simulations were run over 5-nanoseconds (5000 picoseconds), with a 0.001 picosecond time step between energy recalculations. Information about the energy calculations and succeeding structural changes were saved in a data viewer every picosecond. The entire 5 nanosecond run involved one nanosecond of steadily heating the system from 25°C to 75°C, followed by 3 nanoseconds of trajectories, and finally one nanosecond of cooling. All simulations were done under NPT conditions, an abbreviation that stands for constant number of atoms, constant pressure and constant volume.

At the end of the simulations for mutated dimers, the point of minimal energy in the entire 5-nanosecond trajectory was found and compared to energy data collected from simulations of a wild-type A β ₁₆₋₂₂ dimer. The difference seen

in energy minimization during the run should let us know if the mutant is more stable in the parallel β -sheet state than the wild-type peptide.

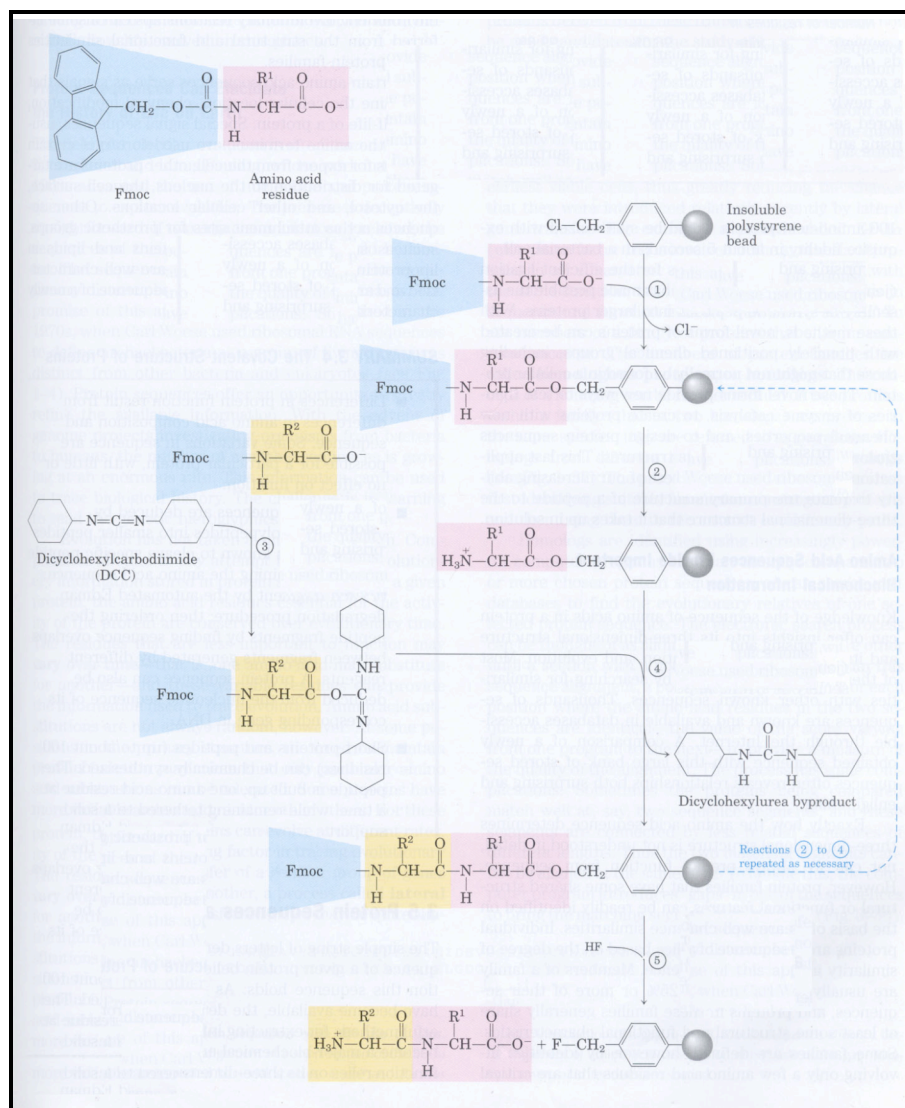


Figure 2.1 – Solid Phase Peptide Synthesis. Fmoc-protected amino acids are added sequentially to an insoluble resin support, with activators and cleavage molecules facilitating the process. [1]

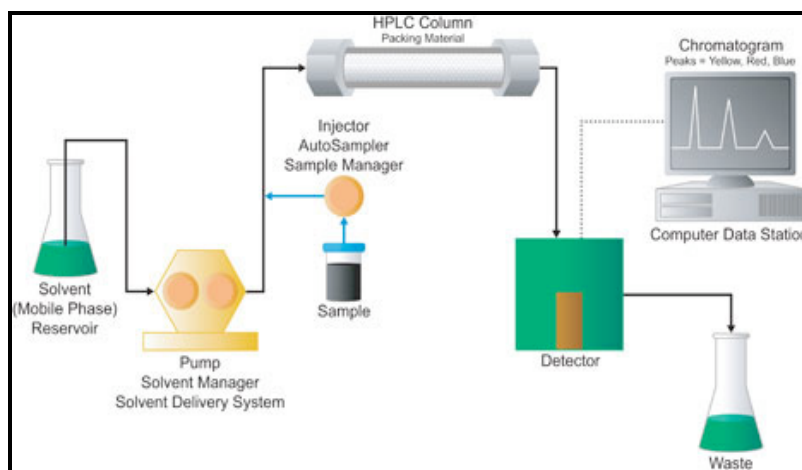


Figure 2.2 – High Performance Liquid Chromatography. The peptide is injected with the mobile phase into the column by the solvent manager pump. From there, increasing amounts of acetonitrile (buffer B) is added to the mobile phase until the peptide sample detaches from the column, and the eluting peptide is detected and measured by the chromatogram as it leaves the column. [39]

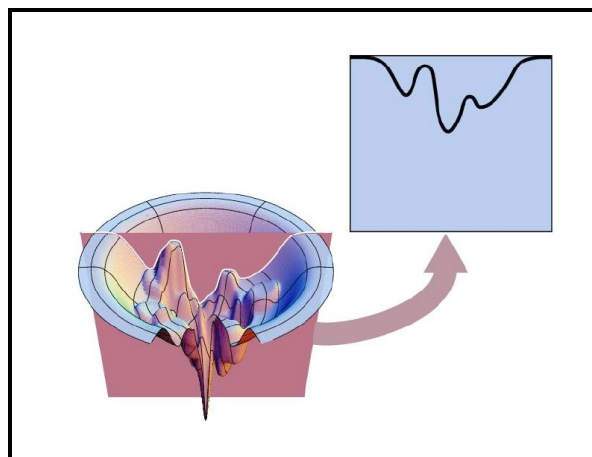


Figure 2.4 – Three-dimensional and one-dimensional depictions of the available energy landscape for a molecular system. The funnel (left) represents the global energy landscape for the system at all available conformations, with the global energy minimum depicting the most stable conformation at the bottom of the funnel. The one-dimensional cross-section of the funnel (right) represents a local energy landscape for the system given its environmental and conformational constraints. The lowest point in the cross-section represents a local energy minimum in the landscape. [40]

$$\begin{aligned}
V(r) = & \sum_{\text{bonds}} K_b (b - b_0)^2 + \sum_{\text{angles}} K_\theta (\theta - \theta_0)^2 \\
& + \sum_{\text{dihedrals}} K_\chi (1 + \cos(n\chi - \delta)) \\
& + \sum_{\text{Urey-Bradley}} K_{UB} (S - S_0)^2 \\
& + \sum_{\text{impropers}} K_\phi (\phi - \phi_0)^2 + \sum_{\text{nonbonded atom pairs}} \\
& \left(\epsilon_{ij} \left[\left(\frac{R_{\text{min},ij}}{r_{ij}} \right)^{12} - \left(\frac{R_{\text{min},ij}}{r_{ij}} \right)^6 \right] + \frac{q_i q_j}{\epsilon_D r_{ij}} \right)
\end{aligned}$$

Figure 2.3 – The potential function for the CHARMM27 force field. K_b , K_θ , K_χ , K_{UB} , and K_ϕ are the bond, valence angle, Urey-Bradley, dihedral angle, and improper dihedral angle force constants, respectively. b , θ , χ , S , ϕ , and are the bond length, bond angle, Urey-Bradley 1,3 distance, dihedral torsion angle, and improper dihedral angle, respectively. The subscript zero represents the starting values for each term at the beginning of the time step at hand during the trajectory. [38]

Chapter 3: RESULTS

Peptide Synthesis and Peptide Purification

There are seven amino acid residues in the A β ₁₆₋₂₂ peptide, and each one was mutated to either asparagine or glutamine amino acids. A total of 11 A β ₁₆₋₂₂ peptide derivatives were synthesized for this study (**Table 3.1**).

All peptides were purified with reverse-phase high performance liquid chromatography. A 0.1% TFA acetonitrile solution (B) was added with increasing concentration to the 0.1% TFA water solution in the mobile phase in order to elute the peptide from the column. Results indicate that the peptides eluted with a range of ~22–28% B, with different percentages occurring with different residue mutations (**Table 3.2**). The absorbance at 220 nm of the exiting mobile phase was used to detect the peptide elution from the column. Peptide absorbance peak intensities ranged from 2000–3000 mAU (**Figure 3.1**).

Mass Spectrometry

The 11 peptides synthesized and purified for this study were analyzed with mass spectrometry to determine the mass-to-charge ratio (**Figure 3.2**). These results were compared with the molecular mass provided in the synthesis records, which indicated the proper molecular mass for all the synthesized peptides (**Table 3.3**).

Deuterium Exchange

All peptides dissolved in the exchange buffer, 0.05M DCl in D₂O, upon sonication except for the E22N mutant, which formed a thick, cloudy gel within 5 minutes of suspension during the first attempt. To dissolve this peptide, it was mixed with 1 mL hexafluoroisopropanol (HFIP), a molecule that helps break up aggregated peptides. While exchange occurred to a large degree before lyophilization, the process was not totally complete at the time of FTIR measurement.

Fourier Transform Infrared Spectroscopy

FTIR scans of the D₂O-exchanged peptides were taken in 1 mM potassium phosphate D₂O buffer from 25°C – 75°C in 10°C increments upon cooling to 25°C. Most spectra contained a small, broad peak at ~1550 cm⁻¹ (not shown in figures) that diminished as the temperature raised and did not return upon cooling. This peak is the result of incomplete H/D exchange within the samples before the spectra were taken; its disappearance is the result of the O–H vibrational mode shifting to a lower frequency as exchange happened over time. Additionally, all spectra in this study show an isosbestic point upon sample heating, which suggests that structural changes from one state to another occurred with no intermediate structure.

As shown in previous FTIR studies, the wild-type A β_{16-22} peptides arrange themselves in antiparallel β -sheets (**Figure 3.3**) [20]. These β -sheets are thermostable, a quality seen by the preservation of amide I' bands in the FTIR

spectrum upon sample heating. The following sections describe the amide I' bands in the spectra for peptides mutated with asparagine and glutamine.

FTIR Results for Asparagine Mutants of A β ₁₆₋₂₂

A total of six different A β ₁₆₋₂₂ peptide derivatives with asparagine mutations were examined. The peptides were mutated at positions 17, 18, 19, 20, 21 and 22 in the A β ₁₆₋₂₂ sequence.

Spectra results for samples mutated at position 22, Ac-KLVFFAN-NH₂, or “E22N”, reveal a sharp amide I' band at 1620 cm⁻¹ at 25°C, with a highly resolved amide I' band component seen at 1687 cm⁻¹. The large separation of the two amide I' band components indicates the peptides form antiparallel β -sheets as opposed to parallel at 25°C. (**Figure 3.9**).

Other than the E22N mutant, asparagine-mutated peptides examined in this work give amide I' bands indicative of parallel β -sheets at 25°C. The spectra for the “L17N” mutant of A β ₁₆₋₂₂ (Ac-KNVFFAE-NH₂; **Figure 3.4**) reveal an amide I' band that appears as a sharp peak at 1621 cm⁻¹ and a less resolved peak at 1636 cm⁻¹, indicative of parallel β -sheet conformation. These peaks are present at these same frequencies at 25 °C in the V18Q mutant (Ac-KLNFFAE-NH₂; **Figure 3.5**) and the F19N mutant (Ac-KLVNFAE-NH₂; **Figure 3.6**). The spectra for samples with asparagine mutations at position 20 (Ac-KLVFNAE-NH₂; **Figure 3.7**) and position 21 (Ac-KLVFFNE-NH₂; **Figure 3.8**) also have the smaller less resolved component of the amide I' band present at 1636 cm⁻¹, but

show the larger amide I' band component at lower (1619 cm^{-1}) and higher (1624 cm^{-1}) wavenumbers, respectively.

In addition to the amide I' bands, all peptides mutated with asparagine showed a peak at $\sim 1660\text{ cm}^{-1}$ representing the vibration of the asparagine side chain carbonyl group. The resolution of this peak depended on the thermostability of each mutant. Also, the peptide samples measured at higher relative concentrations, determined by the overall absorbance intensities of the band components at 25°C , provide more resolved visualization of the side chain peak. The most resolved asparagine side chain peaks are seen in the L17N and A21N mutants.

Increasing the temperature during FTIR experiments determines the relative thermostability among the $\text{A}\beta_{16-22}$ mutant β -sheets. Peptides most stable in the β -sheet conformation retain the amide I' band peaks as the temperature rises. Those that are less stable will lose the β -sheet structure in favor of a random coil state, seen as a broad, rising peak at 1650 cm^{-1} that corresponds to decreasing amide I' bands as temperature increases.

The most thermostable β -sheets of asparagine-mutated $\text{A}\beta_{16-22}$ peptides in this study were seen in L17N, V18N, A21N and E22N. In the L17N spectra, the larger amide I' peak decreased in intensity from 1.36 to 1.26 (a percent difference, Δ , of -7.35%), while its smaller amide I' shoulder shifted slightly to a higher wavenumber of $\sim 1638\text{ cm}^{-1}$ upon heating to 75°C . While a broad random coil rise at $\sim 1650\text{ cm}^{-1}$ was slowly introduced, obscuring the asparagine side chain peak

slightly, it never became fully resolved from the large amide I' band because its intensity only reached ~ 0.5 throughout the temperature rise. A similar situation occurred for the V18N mutant; as the temperature increased to 75°C during the experiment, the large amide I' band peak decreased in intensity from 1.85 to 0.87 ($\Delta = -52.9\%$), the smaller amide I' component from 0.72 to 0.52 ($\Delta = -27.8\%$), and the asparagine side chain band at 1660 cm^{-1} was obscured slightly by the broad random coil rise with an intensity of ~ 0.3 centered around 1650 cm^{-1} . The A21N mutant showed more thermostability in that only the large amide I' band component showed a decrease in intensity, from 1.25 to 1.12 ($\Delta = -10.4\%$), as the sample was heated to 75°C. There was a very small rise ($\Delta < +5\%$) in intensity near the asparagine side chain band at $\sim 1655\text{ cm}^{-1}$, corresponding to some random coil introduction in the sample. The E22N mutant displayed similar relative thermostability upon heating to 75°C, as its spectra showed a decrease of only the large amide I' band, from 0.64 to 0.57 ($\Delta = -10.9\%$), as a slight rise in the slope between the two amide I' bands at $\sim 1650\text{ cm}^{-1}$ (less than 0.05) occurred.

The least thermostable β -sheets of asparagine-mutated $A\beta_{16-22}$ peptides in this study were in mutants that replaced phenylalanine residues. The spectra of the F20N mutant showed a decrease in intensity of the large amide I' component from 0.62 to 0.34 ($\Delta = -45.2\%$) upon heating to 75°C, with a broad random coil band appearing at 1650 cm^{-1} and increasing in intensity from 0.20 to 0.30 ($\Delta = +50.0\%$). The amide I' band remained the highest peak in the spectrum throughout heating, but the random coil band was well-resolved nonetheless; it

was present even at 25°C as a broadening shoulder to the larger amide I' band. In the spectra of the F19N mutant, the absorbance intensity of the large amide I' band component decreased from 0.72 to 0.32 ($\Delta = -55.6\%$) as the sample was heated to 75°C in favor of a large, broad peak at 1652 cm^{-1} . This random coil band is present as a highly resolved peak at 75°C, with an intensity of 0.44, but existed as a large shoulder to the amide I' band even at 25°C, with an initial intensity of 0.32 ($\Delta = +37.5\%$). At its highest intensity at 75°C, the random coil band completely obscures the smaller amide I' band component at 1636 cm^{-1} , while the larger amide I' band component is present at small enough an intensity to appear as a shoulder to the random coil band. These results suggest that the least thermostable β -sheets of all the asparagine mutants in of $A\beta_{16-22}$ were the F19N parallel β -sheets.

The β -sheet unfolding seen in half of the asparagine-mutated $A\beta_{16-22}$ peptides upon heating is reversible, while the other half of the mutants fail to completely recreate their original β -sheet character. After cooling back to the starting temperature of 25°C, mutants L17N, A21N, and E22N display band intensities similar to those at the start of the experiments, with the exception of the water band at 1550 cm^{-1} that was eliminated after further H/D exchange. In some spectra, the larger amide I' band component appears with a higher intensity after cooling than initially; this observation is attributed to the absence of the water band at 1550 cm^{-1} . Spectra of mutants V18N, F19N and F20N, however, fail to show a restoration of the full intensity of the amide I' band components upon

cooling, despite showing the restoration of the asparagine side chain band (**Figures 3.5, 3.6 and 3.7**).

There were a number of uncharacterized bands seen in the FTIR spectra for the asparagine-mutated A β_{16-22} peptides. A small unidentified peak at ~ 1698 cm^{-1} was seen in the spectra of F19N, while small peaks at 1706 cm^{-1} and 1720 cm^{-1} were noted in the F20N and A21N spectra. Additionally, a low frequency shoulder to the larger amide I' band component, at ~ 1608 cm^{-1} , was seen in the V18N, F19N, F20N and A21N spectra at 25°C ; these shoulders appeared to diminish upon heating to 75°C .

FTIR Results for Glutamine Mutants of A β_{16-22}

A total of five different A β_{16-22} peptide derivatives with glutamine mutations were examined. The peptides were mutated at positions 17, 19, 20, 21 and 22 in the A β_{16-22} sequence.

In contrast to the spectral results for peptides mutated with asparagine, most FTIR spectra for peptides mutated with glutamine show amide I' bands that are indicative of antiparallel β -sheet conformation. Spectra of the L17Q mutant (Ac-KQVFFAE-NH₂; **Figure 3.10**), the A21Q mutant (Ac-KLVFFQE-NH₂; **Figure 3.13**), and the E22Q mutant (Ac-KLVFFAQ-NH₂; **Figure 3.14**) showed the larger amide I' band component as a sharp peak at 1619 cm^{-1} at 25°C , with the smaller amide I' component appearing at 1689 cm^{-1} . The F20Q mutant (Ac-KLVFQAE-NH₂; **Figure 3.12**) had similar antiparallel β -sheet amide I'

band separation at 25°C, with the larger component seen at 1618 cm⁻¹ and the smaller at 1686 cm⁻¹. The only peptide that displayed amide I' bands indicative of parallel β -sheets at 25°C was F19Q (Ac-KLVQFAE-NH₂; **Figure 3.11**), with a larger amide I' band component seen at 1619 cm⁻¹ and a smaller, less resolved amide I' band component at 1636 cm⁻¹. The glutamine side chain carbonyl vibrational mode, at ~1655 cm⁻¹, was seen only in the F19Q samples studied.

The most thermostable glutamine-mutated A β ₁₆₋₂₂ peptides in this study were A21Q and E22Q, whose spectral absorbance intensities changed very little upon heating to 75°C ($\Delta < -5\%$), aside from the disappearance of the water band at 1550 cm⁻¹ (not shown). The larger and smaller amide I' band components in the spectra of the F19Q mutant decreased from 0.46 to 0.31 ($\Delta = -32.6\%$) and from 0.27 to 0.20 ($\Delta = -25.9\%$), respectively, during heating to 75°C. These decreases were accompanied by the rise of a broad random coil band that appeared to be centered at ~1652 cm⁻¹ at 75°C; the glutamine side chain band became obscured by this band as the temperature increased. Results for the F20Q mutant were similar; the larger amide I' band component at 1618 cm⁻¹ decreased in intensity from 0.29 to 0.23 ($\Delta = -20.7\%$) and the smaller component at 1686 cm⁻¹ from 0.037 to 0.034 ($\Delta = -8.11\%$) in favor of a random coil band at 1645 cm⁻¹ that increased in intensity from 0.105 to 0.155 ($\Delta = +47.6\%$) upon heating to 75°C. Spectra for the most thermally unstable mutant, L17Q, showed a steady decrease in the absorbance intensity of the larger amide I' band component, from 0.57 to 0.18 ($\Delta = -68.4\%$), in favor of a broad band at 1648 cm⁻¹ that reaches a

peak intensity of 0.27 from ~ 0.16 ($\Delta = +68.8\%$). Reversibility was seen for β -sheet unfolding in every glutamine-mutated peptide in this study, as seen through the restoration of the amide I' band peaks upon sample cooling to 25°C.

Molecular Dynamics Simulations

Molecular dynamics (MD) simulations were conducted for parallel β -sheet dimers for the L17N and L17Q mutants of A β_{16-22} ; each simulation was 5 ns long, with 1 ns of heated trajectories from 25°C – 75°C, 3 ns of trajectories at 75°C, and 1 ns of cooling trajectories. Although both simulations produced energy values much higher than expected, on the order of 100 kcal/mol upon energy minimization and fluctuating around this level throughout the trajectories, results for the MD simulations reveal lower relative energies in the system overall for the L17N mutant than for the L17Q mutant. Screenshots of low-energy points near the end of the trajectories were taken for both dimers, where it appears that the L17N asparagine side chains form a hydrogen bond together in the dimer, and the L17Q glutamine side chains form a hydrogen bond with their respective peptide backbone in the dimers (**Figure 3.15**).

Table 3.1 – Capped A β_{16-22} peptide derivatives synthesized for this study.

A β_{16-22} Mutant Name	Amino Acid Sequence with Capping
L17N	Ac-KNVFFAE-NH ₂
V18N	Ac-KLNFFAE-NH ₂
F19N	Ac-KLVNFAE-NH ₂
F20N	Ac-KLVFNAE-NH ₂
A21N	Ac-KLVFFNE-NH ₂
E22N	Ac-KLVFFAN-NH ₂
L17Q	Ac-KQVFFAE-NH ₂
F19Q	Ac-KLVQFAE-NH ₂
F20Q	Ac-KLVFQAE-NH ₂
A21Q	Ac-KLVFFQE-NH ₂
E22Q	Ac-KLVFFAQ-NH ₂

Table 3.2 – Percentages of 0.085% TFA acetonitrile content (%B) in the HPLC mobile phase at the time of elution for different A β_{16-22} peptide derivatives during purification.

A β_{16-22} Mutant Name	%B at Time of Elution from HPLC Column
L17N	26.2%
V18N	25.5%
F19N	23.2%
F20N	25.6%
A21N	29.0%
E22N	29.1%
L17Q	26.8%
F19Q	24.7%
F20Q	26.0%
A21Q	26.4%
E22Q	29.4%

Table 3.3 – Mass spectrometry results for each A β_{16-22} derivative as compared to molecular mass records from synthesis.

A β_{16-22} Mutant Name	Molecular Mass Without Capping Groups from SPPS Output (amu)	Charge-to-Mass Ratio from Mass Spectrometry Output	Total Molecular Mass after Capping Group Addition (+ ~43 amu)
L17N	852.97	895.7	895.97
V18N	866.99	909.7	909.99
F19N	818.95	861.6	861.95
F20N	818.95	861.6	861.95
A21N	894.00	937.7	937.00
E22N	837.01	879.7	880.01
L17Q	866.99	909.6	909.99
F19Q	832.98	875.6	875.98
F20Q	832.98	875.6	875.98
A21Q	909.70	951.5	952.70
E22Q	851.04	893.6	894.04

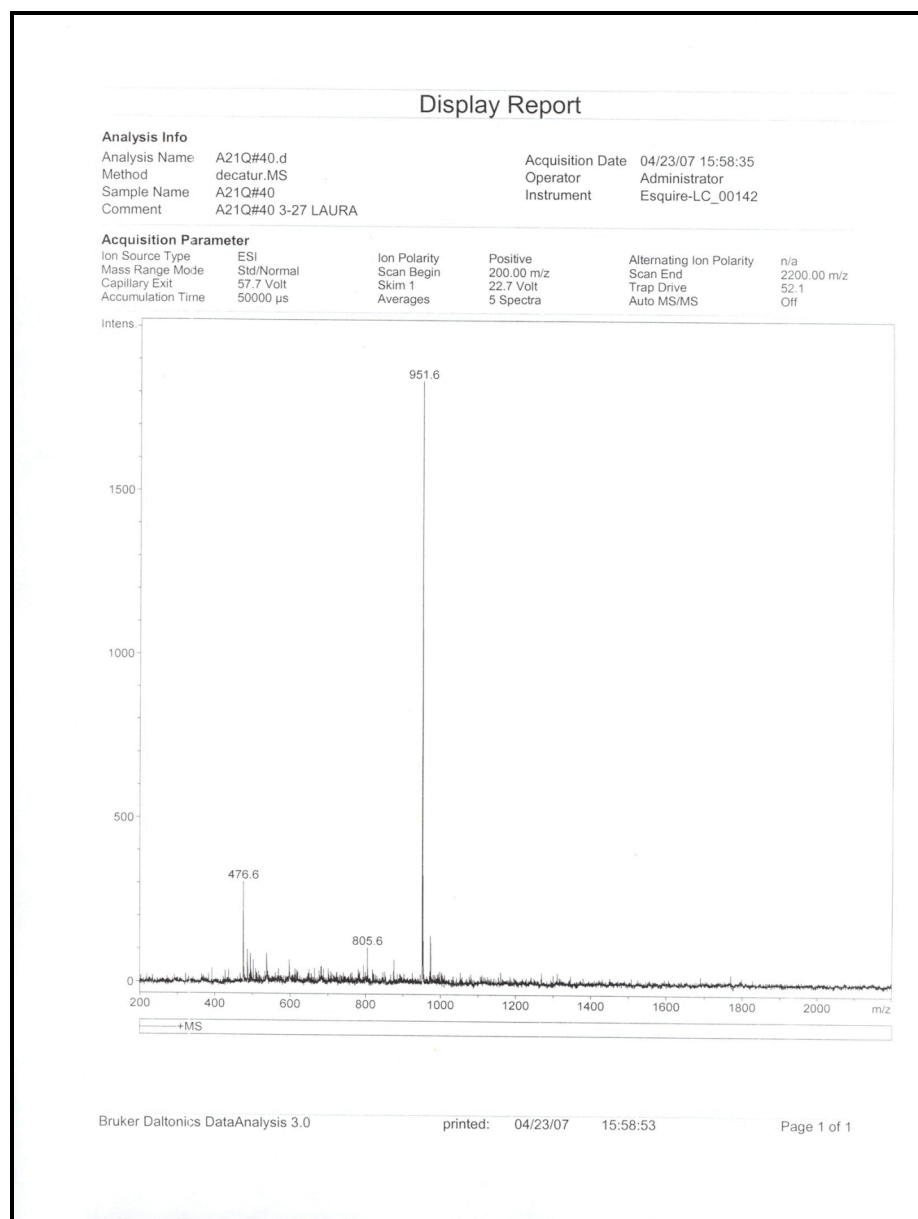


Figure 3.2 – The mass spectrometry output of the A β ₁₆₋₂₂ A21Q mutant. The largest peak reflects the correct mass-to-charge ratio of the peptide synthesized.

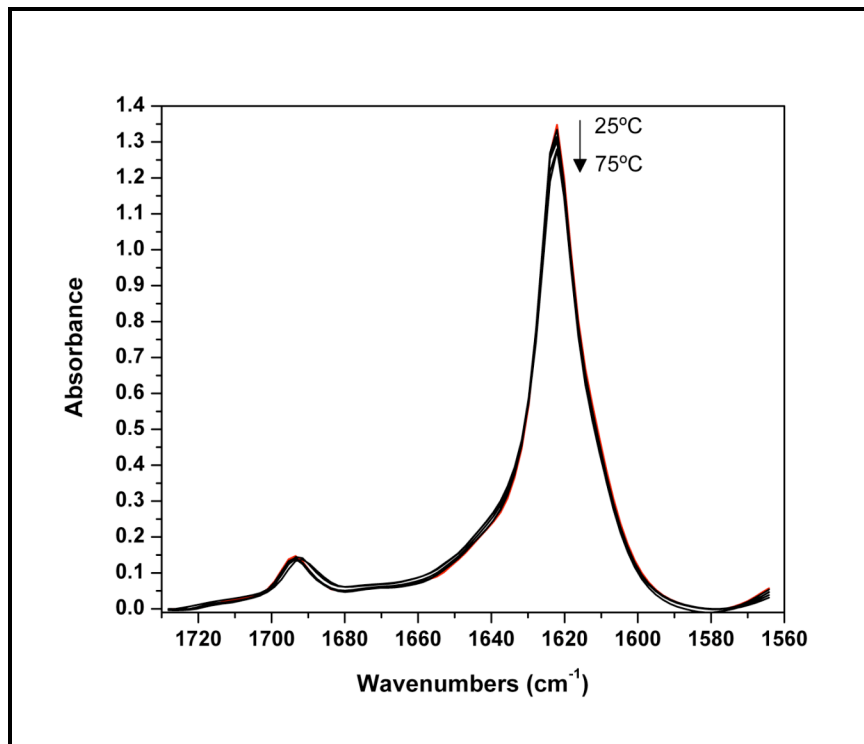


Figure 3.3 – FTIR spectra of the wild-type A β ₁₆₋₂₂ polypeptide. Spectra were taken in 10°C increments from 25°C–75°C and upon cooling to 25°C (represented in red). Arrows indicate areas of the spectra that change in absorbance intensity during heating.

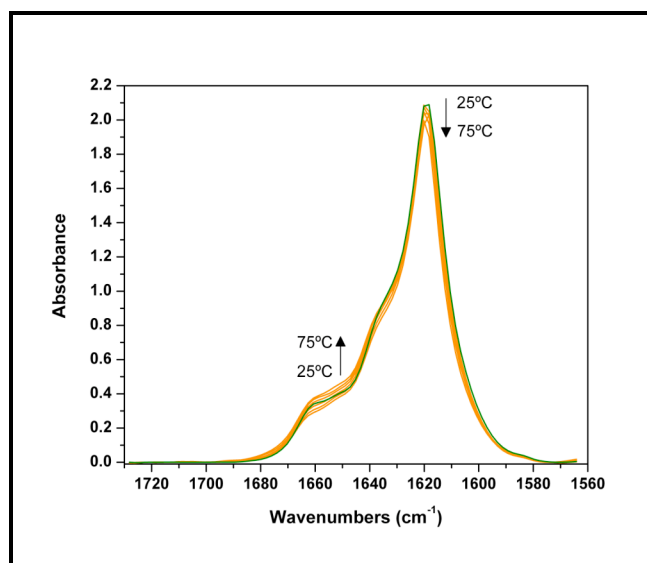


Figure 3.4 – FTIR spectra of the A β ₁₆₋₂₂ mutant L17N. Spectra were taken in 10°C increments from 25°C–75°C and upon re-cooling to 25°C (represented in green). Arrows indicate areas of the spectra that change in absorbance intensity during heating.

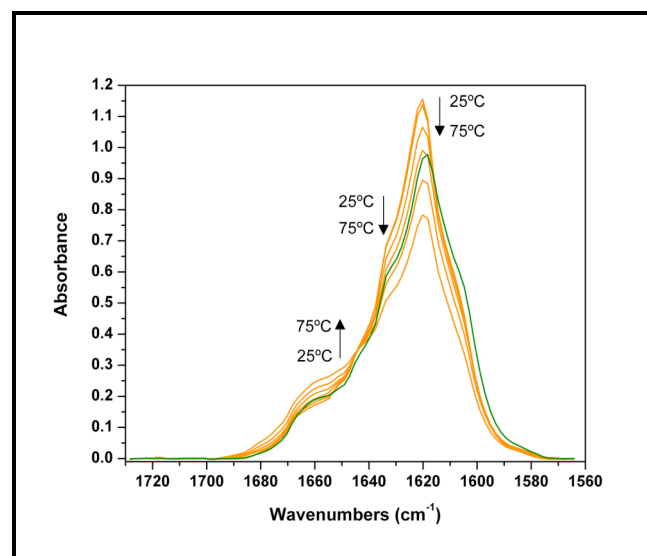


Figure 3.5 – FTIR spectra of the A β ₁₆₋₂₂ mutant V18N. Spectra were taken in 10°C increments from 25°C–75°C and upon re-cooling to 25°C (represented in green). Arrows indicate areas of the spectra that change in absorbance intensity during heating.

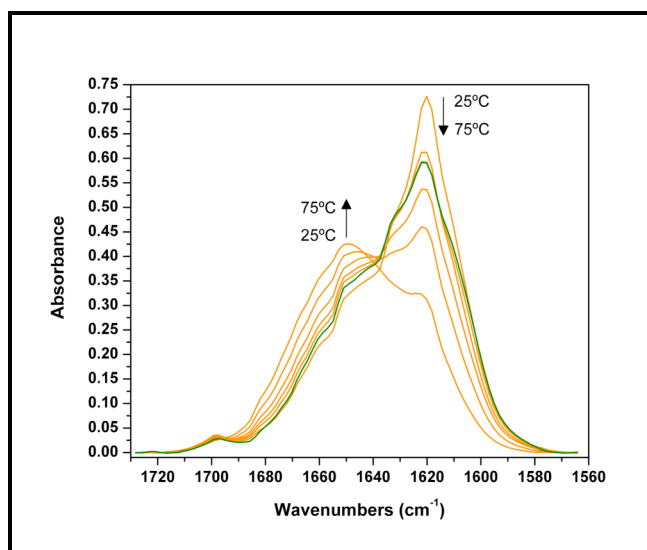


Figure 3.6 – FTIR spectra of the Aβ₁₆₋₂₂ mutant F19N. Spectra were taken in 10°C increments from 25°C–75°C and upon re-cooling to 25°C (represented in green). Arrows indicate areas of the spectra that change in absorbance intensity during heating.

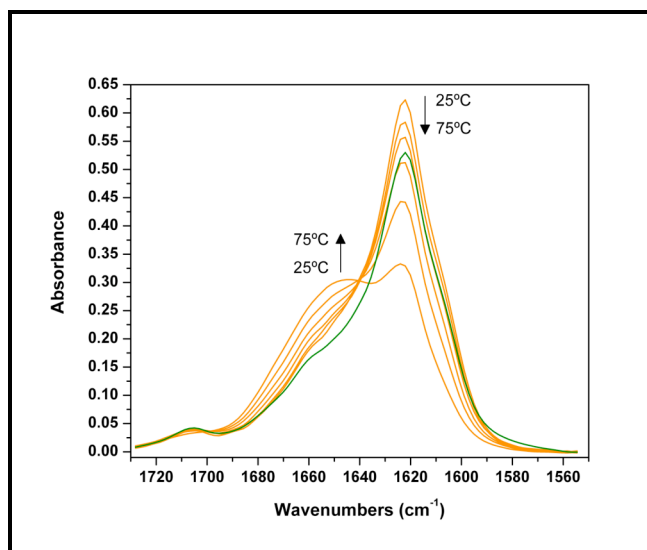


Figure 3.7 – FTIR spectra of the Aβ₁₆₋₂₂ mutant F20N. Spectra were taken in 10°C increments from 25°C–75°C and upon re-cooling to 25°C. Arrows indicate areas of the spectra that change in absorbance intensity during heating.

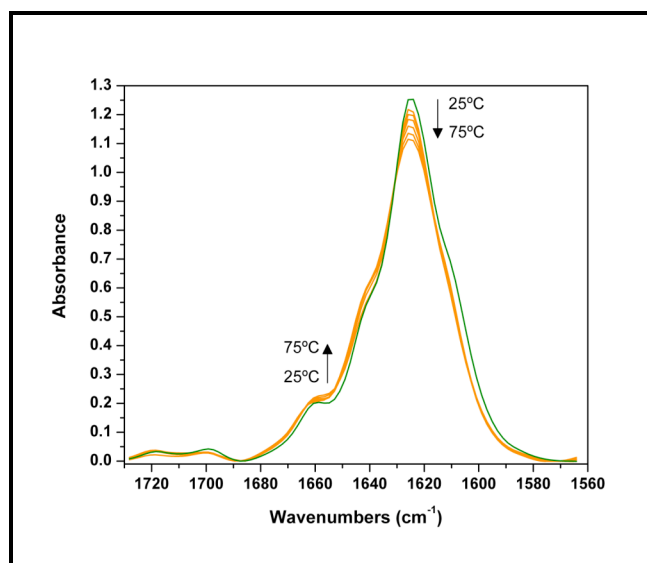


Figure 3.8 – FTIR spectra of the Aβ₁₆₋₂₂ mutant A21N. Spectra were taken in 10°C increments from 25°C–75°C and upon re-cooling to 25°C (represented in green). Arrows indicate areas of the spectra that change in absorbance intensity during heating.

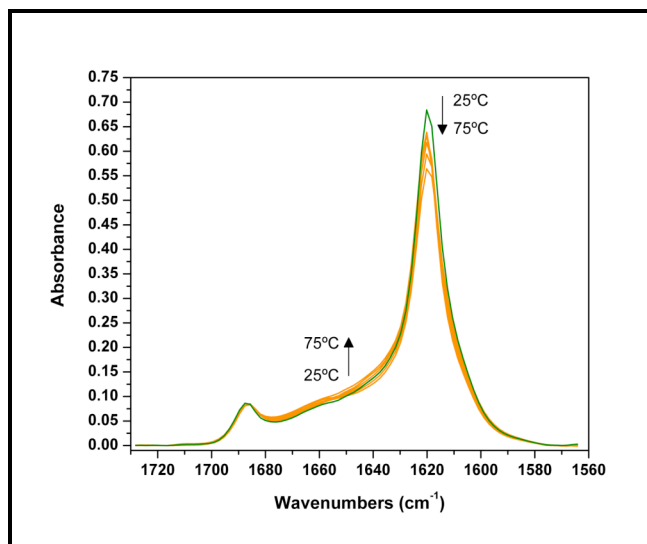


Figure 3.9 – FTIR spectra of the Aβ₁₆₋₂₂ mutant E22N. Spectra were taken in 10°C increments from 25°C–75°C and upon re-cooling to 25°C (represented in green). Arrows indicate areas of the spectra that change in absorbance intensity during heating.

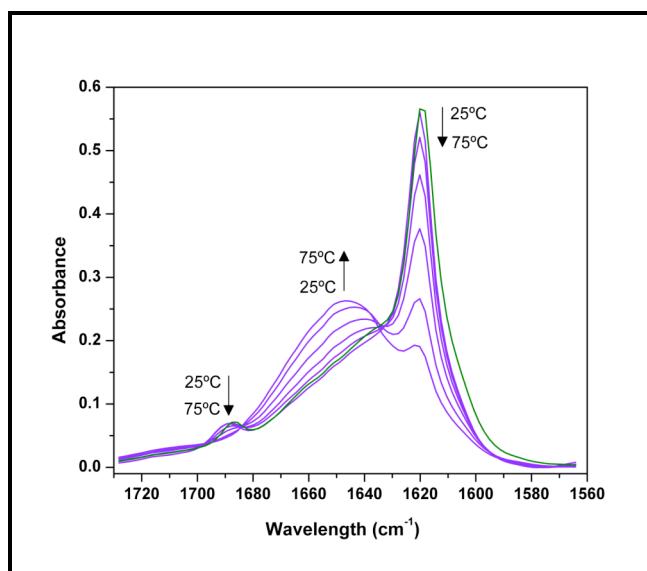


Figure 3.10 – FTIR spectra of the A β ₁₆₋₂₂ mutant L17Q. Spectra were taken in 10°C increments from 25°C–75°C and upon re-cooling to 25°C (represented in green). Arrows indicate areas of the spectra that change in absorbance intensity during heating.

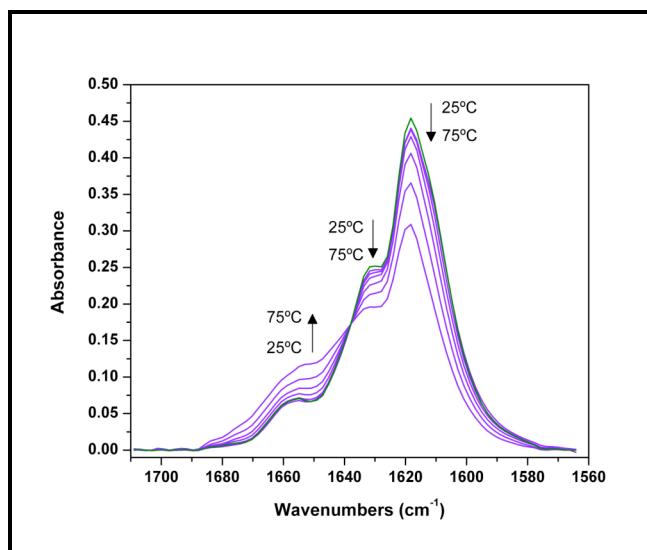


Figure 3.11 – FTIR spectra of the A β ₁₆₋₂₂ mutant F19Q. Spectra were taken in 10°C increments from 25°C–75°C and upon re-cooling to 25°C (represented in green). Arrows indicate areas of the spectra that change in absorbance intensity during heating.

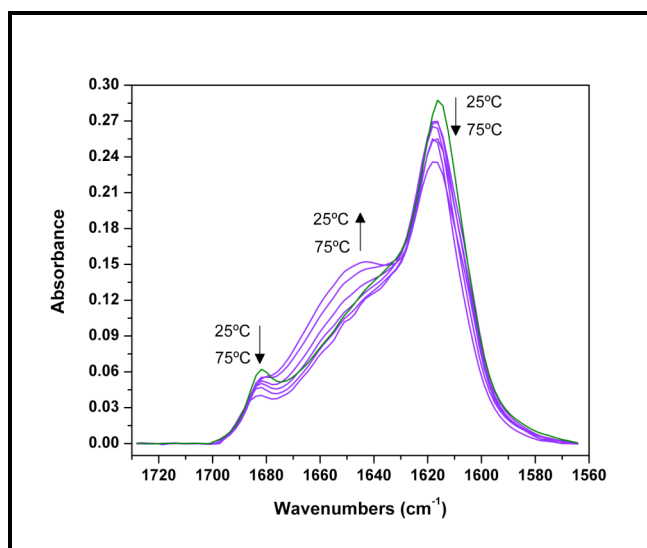


Figure 3.12 – FTIR spectra of the Aβ₁₆₋₂₂ mutant F20Q. Spectra were taken in 10°C increments from 25°C–75°C and upon re-cooling to 25°C (represented in green). Arrows indicate areas of the spectra that change in absorbance intensity during heating.

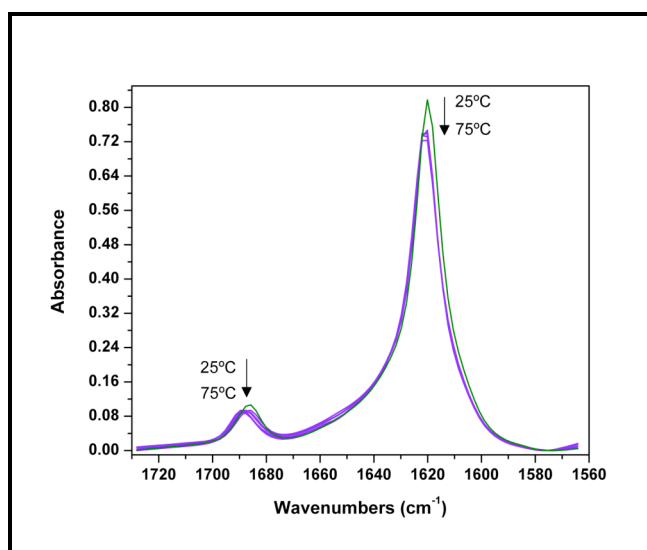


Figure 3.13 – FTIR spectra of the Aβ₁₆₋₂₂ mutant A21Q. Spectra were taken in 10°C increments from 25°C–75°C and upon re-cooling to 25°C (represented in green). Arrows indicate areas of the spectra that change in absorbance intensity during heating.

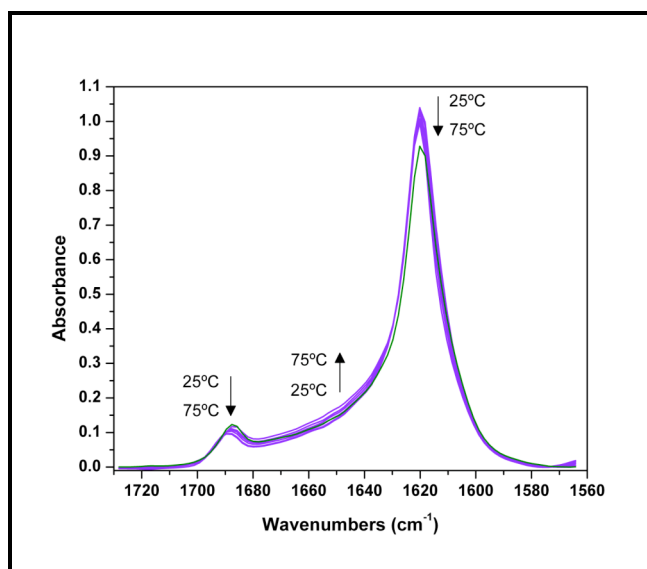
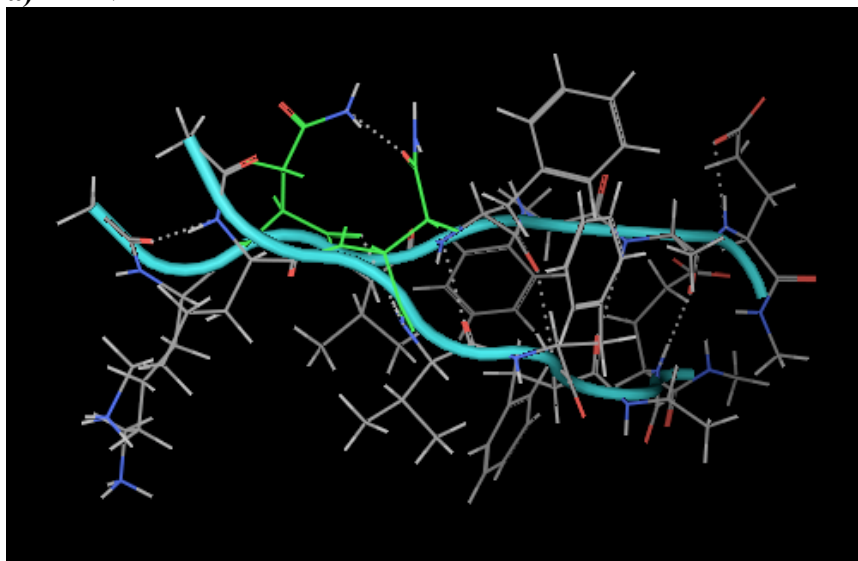


Figure 3.14 – FTIR spectra of the Aβ₁₆₋₂₂ mutant E22Q. Spectra were taken in 10°C increments from 25°C–75°C and upon re-cooling to 25°C (represented in green). Arrows indicate areas of the spectra that change in absorbance intensity during heating.

a) L17N



b) L17Q

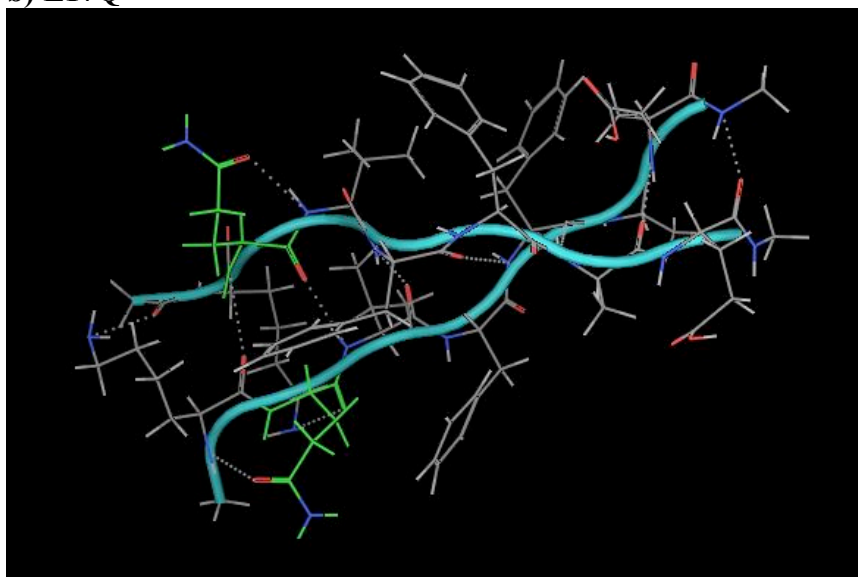


Figure 3.15 – Screenshots from the Molecular Operating Environment computer program of the L17N (a) and L17Q (b) mutants of Aβ₁₆₋₂₂. The backbones for each dimer are highlighted in aqua, and the mutated residue is highlighted in green for each image; (A) is asparagine, and (B) is glutamine. Nitrogen atoms are shown in blue, oxygen atoms in red, carbon atoms in grey and hydrogen atoms in white. Hydrogen bonds are depicted as a grey dotted line.

Chapter 4: DISCUSSION

Peptide Synthesis, Purification and Preparation

In general, the 11 peptides prepared for this study had similar yields after synthesis. Each synthesis produced approximately 20 milligrams of crude peptide after cold ether precipitation and lyophilization, and each crude sample easily dissolved in a solution of four milliliters of 0.1% TFA distilled water and 0.5 milliliters of 0.085% TFA acetonitrile preceding purification. The HPLC data chromatogram revealed a peptide peak at 222 nm with an intensity of ~2700 mAU for every peptide except F20N and F20Q, when an intensity of ~1500 mAU was observed. These lower intensities suggest that the peptides eluted from the column at a lower concentration than the other peptides, which implies that they were synthesized with a lower yield. The mass spectrometry results for the peptides verified the expected mass-to-charge ratio for the purified peptides.

Purified peptides utilized in FTIR analysis were exposed to H/D exchange prior to measurements. Every peptide sample except one readily dissolved in at least two milliliters of 0.5M DCl in D₂O. The peptide that did not dissolve was E22N; upon exposure to the exchange buffer, this peptide appeared to aggregate, thickening over a period of six hours to form a cloudy gel. The problem was corrected during the second attempt at exchange, when another E22N sample was

exposed to hexafluoroisopropanol to help discourage the formation of insoluble aggregates. It is possible, due to the position of the asparagine mutation in the A β_{16-22} peptide sequence, that the E22N peptide forms stable aggregates more readily than other mutated samples. Spectral information from subsequent FTIR studies probes this possibility further.

Fourier Transform Infrared Spectroscopy

Based on the presence of two amide I' bands in FTIR spectra for every peptide, a larger component with a lower frequency of $\sim 1620\text{ cm}^{-1}$ and a smaller component with a higher frequency of either $\sim 1636\text{ cm}^{-1}$ or $\sim 1690\text{ cm}^{-1}$, we can conclude that neither asparagine nor glutamine single-residue mutations prevent the formation of amyloid aggregates in the A β_{16-22} peptide. This finding suggests that the formation of intermolecular β -sheets, the most stable secondary structure in the A β_{16-22} peptide, does not depend on any particular residue in the sequence alone. Various interactions among these residues act together to facilitate the energetic stability of this conformation, and despite the possibility that certain interactions may carry more weight overall, none of them is an absolute deciding factor in β -sheet formation.

The notion that the entire peptide sequence acts together to promote β -sheet formation in A β_{16-22} is most likely a consequence of the hydrophobic nature of most of the residues in the sequence. Leucine, valine, phenylalanine and alanine are all hydrophobic physically and do not associate with polar molecules.

Because these residues are not soluble in water, but can interact well with other hydrophobic residues based on van der Waals' interactions, they may "seek out" other peptides in the solution and create β -sheets as a way to avoid interaction with polar molecules.

The tendency of the largely hydrophobic characteristics of the $A\beta_{16-22}$ peptide, and those of its asparagine/glutamine mutants, to promote β -sheet formation is clear-cut physically and supported by our data. Normally, the $A\beta_{16-22}$ peptide forms thermostable, antiparallel β -sheets, an orientation largely attributed to the encouragement of electrostatic attractions between the charged lysine and glutamic acid residues that flank the peptide's hydrophobic core (**Figure 4.1**). We found in this study, however, that substituting almost any position in the $A\beta_{16-22}$ peptide with asparagine causes the β -sheets to align in a parallel orientation, the thermostability of which depends on the position changed. Strangely enough, this conversion to parallel β -sheets is not seen with most glutamine mutations, despite the fact that side chains in asparagine and glutamine amino acids have the same terminal functional group and differ only by one CH_2 group near the base of the chain.

Asparagine Mutants of $A\beta_{16-22}$ Form Mainly Parallel β -Sheets

We learned in this study, based on amide I' band positions in the FTIR spectra of asparagine-mutated $A\beta_{16-22}$, that the changes in sequence in nearly every position of the peptide promoted the formation of parallel β -sheets. Spectra

at 25°C for L17N, V18N, F19N, F20N and A21N samples all produced a sharp amide I' band component at $\sim 1620\text{ cm}^{-1}$ with a poorly resolved, less intense component at $\sim 1636\text{ cm}^{-1}$; these results contrast with those from FTIR studies of the wild-type peptide, which forms stable antiparallel β -sheets. The one exception to the parallel trend in asparagine mutants is E22N, which produced amide I' bands at $\sim 1620\text{ cm}^{-1}$ and $\sim 1690\text{ cm}^{-1}$, indicating the presence of antiparallel β -sheets.

A number of structural features of asparagine mutants of $A\beta_{16-22}$ can account for the change in β -sheet orientation. One aspect involves the ability of an asparagine side chain to form a hydrogen bond with another asparagine side chain. Assuming the peptides are in-register when they form parallel β -sheets, the asparagine residues from different peptides are able to hydrogen bond together across the strands, stabilizing the β -sheets in a parallel conformation (**Figure 4.2**). The Asn-Asn interaction would be impossible in an antiparallel β -sheet orientation because the residues would be too far apart from each other to form hydrogen bonds, and none of the other residues in the rest of the sequence has a hydrogen bond donor or acceptor in the side chain, so the asparagine side chains would be unable to form hydrogen bonds with any other residue. Hydrogen bonds are fairly strong non-covalent interactions, and when present in large numbers, they account for much of the stability proteins have upon folding into specific conformations. Therefore, the opportunity for asparagine side chains to hydrogen

bond together in large numbers within a multi-peptide β -sheet may give the parallel conformation enough stability to be preferred overall.

Another feature of the A β_{16-22} peptide sequence that may account for the stability of parallel asparagine mutants is the presence of two central phenylalanine residues in the peptide sequence whose aromatic rings can facilitate π - π electron van der Waals' interactions across strands. When oriented as in register parallel β -sheets, the two phenylalanine residues at positions 19 and 20 in the peptide sequence can stack favorably with those in adjacent strands. Peptides arranged as in-register antiparallel β -sheets allow for only the phenylalanine residues at position 19 to stack favorably with one another in adjacent strands (**Figure 4.3**). Like hydrogen bonds, van der Waals' interactions can be strong in large numbers within a molecular system, and so the two-fold addition of phenylalanine ring stacking could provide a significant amount of stability to the peptides when oriented as parallel β -sheets. This stability, accompanied by the stability offered from asparagine side-chain hydrogen bonding, may tip the energetic scale in favor of parallel β -sheets for most mutants at 25°C.

Despite the stability of asparagine hydrogen bonding, there remains the issue of electrostatic repulsions between lysine and glutamic acid side chains in parallel β -sheets. Lysine and glutamic acid side chains are positively and negatively charged at neutral pH according to the pKa values of their side chains (10.53 and 4.25, respectively) [1]. The columbic repulsion experienced by these two charged residues at a large scale in parallel β -sheets would certainly

outweigh the energetic benefits that arise from increased hydrogen bonding and van der Waals' interactions. To combat this repulsion problem, it is possible that asparagine-mutated $A\beta_{16-22}$ peptides form β -sheets that are parallel in conformation but stacked upon each other in an antiparallel fashion. The result is akin to a stacked β -sheet sandwich, with the β -sheets as "slices" pointing in opposing directions. In this orientation, the positively charged lysine residues from one parallel β -sheet can interact with the negatively charged glutamic acid residues from another parallel β -sheet.

There is another benefit to β -sheet stacking in addition to quelling electrostatic repulsions between charged residues. Recall the nature of side chains in β -sheets, shown in **Figure 1.7** in the introduction. Each adjacent side chain in a strand points up or down perpendicularly from the backbone strand axis in the opposite direction of its neighbor. While the direction of side chains next to each other in the sequence alternate within one strand, each side chain points in the same direction as those in residues directly across from it in the adjacent strand in a β -sheet, regardless of strand orientation. This pattern creates pleats on the surface of the β -sheets that run perpendicularly from the peptide backbone axis; the raised side chain pleats of one sheet upon stacking fill the pleat valleys devoid of side chains in another sheet. This kind of intersheet stacking is a feature used to describe amyloid fibrils at a large scale; it is an especially useful way to protect hydrophobic residues from exposure to solvent by facilitating additional van der Waals' interactions between intersheet hydrophobic side chains interlocked within

the β -stacks. The increase in hydrophobic side chain contacts and charge neutralization in parallel β -sheets of asparagine mutants lessens the detrimental effect of asparagine's presence within the hydrophobic core of the β -sheets, which would allow the benefits of asparagine hydrogen bonding to have a greater relative impact on secondary structure.

The directionality, and even presence, of β -stacks cannot be detected with infrared spectroscopy methods utilized in this study. The carbonyl groups in the peptide backbone within each β -sheet are in a parallel conformation regardless of the way the sheets face each other in stacks, as they lie in the plane of the β -sheet and not in the plane of the stacks. Thus, the backbone carbonyl groups possess the same transition dipole coupling behavior regardless of the β -stacking orientation, and the amide I' bands seen in FTIR reflect only the orientation of strands within the β -sheets. Therefore, we cannot be sure of the presence of β -stacks in the peptide samples using FTIR alone.

As stated earlier, our results show that there is one exception to the rule of parallel β -sheet formation in A β_{16-22} asparagine peptide mutants; the peptide E22N forms antiparallel β -sheets. The position of this mutation can help explain why the peptide prefers the antiparallel conformation. Asparagine replaces the negatively charged glutamic acid residue in E22N. While the negative charge in the glutamic acid side chain attracts to the lysine positive charge in the wild-type peptide, asparagine in its place still interacts in a stabilizing way with the lysine side chain. The side chain in asparagine is electron-rich and has the potential to

quell the positive charge density surrounding the amide group on the end of the lysine side chain. The position of the E22N mutation also leaves the hydrophobic core of the peptide intact, which helps shield it from polar solvent in a fashion similar to the wild-type A β_{16-22} . Because the E22N mutation best preserves the physical properties of the wild-type peptide, it preserves the antiparallel β -sheet conformation.

Glutamine Mutants of A β_{16-22} Form Mainly Antiparallel β -Sheets

The data collected for A β_{16-22} peptides mutated with glutamine suggest β -sheet orientations that are nearly opposite to those in asparagine mutants. We learned in this study, based on amide I' band positions in the FTIR spectra of glutamine-mutated A β_{16-22} peptides, that the changes in sequence in nearly every position of the peptide maintained the formation of antiparallel β -sheets at 25°C. Spectra at for L17Q, F20Q, A21Q and E22Q samples all produced a sharp amide I' band component at $\sim 1620\text{ cm}^{-1}$ with a highly resolved, less intense component at $\sim 1690\text{ cm}^{-1}$. These room-temperature results agree with those from FTIR studies of the wild-type peptide, which forms stable antiparallel β -sheets, although the stability of the mutated β -sheets is affected at higher temperatures. The one exception to the antiparallel trend in glutamine mutants is F19Q, which produced amide I' bands at $\sim 1620\text{ cm}^{-1}$ and $\sim 1636\text{ cm}^{-1}$, indicating the presence of parallel β -sheets. At first glance, it seems strange that mutating A β_{16-22} with the amino acid most similar to asparagine would result in the formation of

β -sheets with an orientation completely opposite from that of asparagine mutants. These results emphasize the sensitivity of peptide secondary structure to subtle primary sequence changes.

Glutamine has one more CH_2 group in its side chain than does asparagine; they are identical otherwise. Two consequences of the increased side chain length in glutamine over asparagine may account for the switch in β -sheet orientation between peptides mutated with these residues. The extra CH_2 link gives the glutamine side chain a higher degree of torsional freedom than the asparagine side chain (**Figure 1.10**). Although they share the same functional amide group, allowing two glutamine residues to form a hydrogen bond between amide side chain groups just as two asparagine residues can, there is a greater entropic loss when glutamine side chains hydrogen bond (**Figure 4.4**). Thermodynamic equilibrium is a balance between energy minimization and entropy maximization, so this loss of entropy upon glutamine hydrogen bonding may override the benefits of glutamine hydrogen bonding, driving the peptides to form antiparallel β -sheets. The other consequence of the increased side chain length in glutamine is the residue's improved hydrophobic compatibility relative to asparagine. The polar amide group on glutamine can extend farther away from the hydrophobic residues nearby in the sequence of $\text{A}\beta_{16-22}$ than that of asparagine, so it has less of a tendency to interact negatively with the hydrophobic side chains. This opens up an opportunity for the hydrophobic alkyl chain that leads up to the functional group in glutamine to help stabilize the other hydrophobic residues, more closely

resembling the wild-type environment. These energetic benefits are only valid when the residue is free of side chain constraints; if it were hydrogen bonded with another glutamine side chain, as would be the case in parallel β -sheets, the glutamine residue would be forced to bend inward, possibly destabilizing the hydrophobic residues with its polar functional group. The fact that glutamine is just a bit longer than asparagine consequently provides both entropic and energetic benefits for antiparallel β -sheet conformation in glutamine mutants of $A\beta_{16-22}$.

The conformational entropy and hydrophobic limitations of glutamine residues in parallel β -sheets of $A\beta_{16-22}$ mutants are not the only aspects that may be driving these peptides toward antiparallel β -sheet conformation. There are also electrostatic attractions that are optimized between lysine and glutamic acid when the peptides are oriented as antiparallel β -sheets. Electrostatics are significant non-covalent interactions between atoms and contribute much to the energetic stabilization of the wild-type $A\beta_{16-22}$ peptides. If glutamine side chain hydrogen bonding and subsequent double Phe-Phe stacking in parallel β -sheets do not energetically justify reorganizing β -stacks in antiparallel, then the process should not happen, and the peptides should take the path of least resistance toward antiparallel β -sheets.

The one exception to the trend of antiparallel β -sheet formation in glutamine-mutated $A\beta_{16-22}$ peptides in our study is F19Q, which produced amide I' bands in FTIR that were indicative of parallel β -sheet. Recognizing that

position 19 is the exact center of the seven-residue peptide makes the reasons behind this change in orientation clearer. Normally, a phenylalanine residue occupies the central position 19 in $A\beta_{16-22}$, so no matter the orientation of β -sheets, the stabilizing aromatic ring stacking can occur between strands in the β -sheets. When glutamine is introduced in this position, the ring stacking no longer occurs here. A way to restore the stability lost upon phenylalanine-to-glutamine mutation at position 19 may be to orient the β -sheets in a parallel fashion, allowing the phenylalanine residues at position 20 to align and create ring stacking. The energetic benefits from forming these parallel β -sheets, along with possible antiparallel β -stacking as discussed in the previous section, may outweigh the energetic and entropic detriments created with glutamine side chain hydrogen bonding at this unique position in the $A\beta_{16-22}$ peptide.

Effects of Mutations on the Thermal Stability of $A\beta_{16-22}$

Almost all of the position mutations within $A\beta_{16-22}$ caused β -sheet instability compared to the wild-type peptide based on the temperature-controlled FTIR results, and the degree of instability depended on the mutation position.

The only mutant that completely preserved its original 25°C spectra up to 75°C was the antiparallel A21Q. Its asparagine counterpart, parallel A21N, was the most thermostable of all the asparagine mutants, with a 10.4% decrease in the absorbance intensity of the large amide I' band component as the temperature increased. We speculate that the hydrophobic alanine side chain does not

contribute much to the thermodynamic environment in the peptide because it is very small and cannot interact well with other residue side chains. Replacing alanine will therefore have the least detrimental impact on the stability of the peptide, no matter the orientation of β -sheets that become preferred with the presence of the new residue, because of its small stabilizing contributions.

The next most stable mutants in $A\beta_{16-22}$ are found at position 22, where antiparallel β -sheets are present for both asparagine and glutamine substitutions. The large amide I' band component for E22N decreases in intensity by 10.9% upon heating to 75°C, while the E22Q mutant amide I' band decreases by less than 5%. The functional amide side chains of asparagine and glutamine have an electron density fairly similar to the carboxyl functional group in the glutamic acid side chain. When glutamic acid is replaced with either of these polar residues, the stabilizing interactions with charged lysine are not totally lost because the carbonyl group on both asparagine and glutamine can hydrogen bond with the amine group on the lysine side chain. While this hydrogen bond is not as stabilizing to lysine as the electrostatic salt bridge from glutamic acid, it does help quell the positive charge on lysine by sharing its electron density through the hydrogen bond. The fact that the glutamine side chain is longer than the asparagine side chain could mean less torsional strains are required by the lysine side chain to create the hydrogen bond with glutamine. This advantage in length could be the reason for the slightly more stable characteristics in E22Q than E22N.

As the mutation positions in $A\beta_{16-22}$ shift more toward the hydrophobic core of the peptide, we see a decrease in the thermostability of the β -sheet conformation. The F20Q and F19Q mutations give rise to larger amide I' bands that decrease 20.7% and 32.6% respectively upon heating, while the F20N and F19N mutants create amide I' bands that decrease 45.2% and 55.6% respectively upon heating. Glutamine mutations at position 20, which deletes a phenylalanine residue in the hydrophobic core, creates antiparallel β -sheets, most likely the result of the entropic benefits of free glutamine side chains winning out over benefits from glutamine side chain hydrogen bonding. Asparagine mutations at position 20 create parallel β -sheets, a change in orientation that occurs most likely to facilitate the stabilizing effects of the asparagine side chain hydrogen bond. Additionally, mutation at position 19 with either residue prevents the only side chain interaction that is conserved in both parallel and antiparallel β -sheets. No matter the reason for strand direction, the presence of these polar side chains in the core of the strands diminishes the hydrophobic differences between the inner and outer residues, a feature that could be the most important driving force toward β -sheet formation overall. Without a strong need to sequester the core residues away from solvent, $A\beta_{16-22}$ peptides would have less of an energetic barrier that forces them to stay as β -sheets in solution, and they may break apart easier in a warmer environment. Asparagine's shorter side chain gives rise to a more polar core, which may explain the larger drop in β -sheets in F20N and F19N when compared to F20Q and F19Q.

The position where asparagine and glutamine mutants differ the most in terms of thermostability is position 17, where a leucine is deleted. L17N mutants create parallel β -sheets that do not break apart very much with an increase in temperature; the larger amide I' component decreases by only about 7.35% upon heating to 75°C. L17Q mutants, on the other hand, create antiparallel sheets that start out with a significant amount of instability, a feature that only increases with temperature. The larger amide I' band in these mutants decreases by 68.4% in favor of a random coil band, already present with high resolution at 25°C, that increases by 68.8% upon heating to 75°C. The difference in stability between these two mutants can be attributed to the orientation in which they form β -sheets to begin with. As discussed before, the parallel orientation of L17N β -sheets probably creates a hydrogen bond between the asparagine side chains. This hydrogen bond can prevent asparagines from withdrawing electrons from the side chain of any glutamic acid residue that may come near them upon antiparallel β -sheet stacking, which may occur to stabilize the charge repulsions caused by the parallel strands. The antiparallel conformation of L17Q, however, provides no such protection of glutamic acid side chains from glutamine. As the strands orient themselves opposite each other, glutamic acid residues line up with lysines to create a stabilizing salt bridge. Additionally, β -sheets could stack on top of one another to help protect the hydrophobic core residues from solvent. If this is happening, one of the charged terminal ends would be forced into close proximity with the glutamine side chain, destabilizing the β -stack. It would not matter

whether the β -stacks are parallel or antiparallel; the glutamic acid side chain has both a hydrogen bond donor (NH_1) and a hydrogen bond acceptor ($\text{C}=\text{O}$), so it can partially neutralize either functional moiety on lysine or glutamic acid with a hydrogen bond and weaken the stabilizing salt bridge usually formed between them. Thus, no matter how the stacks are oriented in L17Q, the antiparallel conformation of strands within the β -sheet could ultimately destabilize the entire β -stacking motif of the amyloidogenic $\text{A}\beta_{16-22}$ peptide. Although we cannot detect β -stacks using techniques in this study, the thermal instability differences seen between L17N and L17Q β -sheets provides an indirect notion of their presence in the samples.

Molecular Dynamics Simulations

Screenshots of low energy points in the molecular dynamics simulations of L17N and L17Q parallel β -sheet dimers showed different behavior between the side chains of mutated residues. These points in the simulations provide visualization of stability differences that are consistent with our FTIR data. The parallel β -sheet L17N mutant dimer in the simulation created hydrogen bonds between the two asparagine side chains, while the parallel β -sheet L17Q mutant dimer showed the glutamine side chains having a greater ability to deviate away from each other, possibly even forming hydrogen bonds with the peptide backbone. L17Q does not form parallel β -sheet *in vitro* in our study, but rather prefers the antiparallel conformation. The fact that the CHARMM27 force field

calculated higher energy levels of the L17Q dimer relative to the L17N dimer when in parallel β -sheet orientation suggests an inherent difference in the way these residues behave in the A β ₁₆₋₂₂ sequence.

Despite having reached this agreeable correlation, there were many problems with the simulations that need to be fixed in order to use them convincingly as anything other than a cartoon schematic of what might be going on. Implicit solvent was used in the system during simulations, a mathematical approximation known to produce conflicting results with simulations that use explicitly placed water molecules [41]. Including explicit water molecules slows down a simulation considerably due to the increased number of interactions that need to be computed individually, but assuming the force field utilized is accurate enough, including the individual water molecules could help to accurately predict the way our peptide side chains interact. Also, our peptide systems would need considerable enlargement in order to give any useful information about specific hydrophobic stabilization. In the current setup, there are only two peptide strands in the β -sheet, so all the residues are forced to interact with the solvent environment. Creating larger β -sheets, perhaps with one or two β -stacks, should give us much more convincing force field information about how at the mutant side chains really interact with other residues. Finally, the problem of the high energy values in both simulations would need to be addressed in order to be sure that the correct potential interactions are being followed in the simulation. The overall energies of both the L17N and L17Q systems were on the order of 100

kcal/mol during the simulations, which suggest that there was some major repulsion or destabilization happening within the dimers. Since the starting coordinates were taken from the PDB and subsequently manipulated to include end capping, it is possible that the program overlapped atoms, which would show up as a large strain in energy on the system. No matter the source, this problem of high energy in each mutant dimer system must be corrected in order to provide realistic information about its behavior.

Conclusions and Future Directions

Our study reveals that even subtle changes within the sequence of the A β ₁₆₋₂₂ peptides can significantly impact how they behave structurally and energetically. Indeed, the seemingly small, and often overlooked, differences between asparagine and glutamine side chains have a distinct effect on the final structural conformation of the A β ₁₆₋₂₂ peptide. The extra CH₂ group in the side chain of glutamine may give it more entropic and hydrophobic weight when considering the thermodynamic equilibrium of the A β ₁₆₋₂₂ peptides, leading to antiparallel β -sheet formation that may allow for more glutamine side chain movement at positions near the ends of the peptides. Conversely, the presence of glutamine at the central position prompts strands to orient parallel to each other to recreate stabilizing ring stacking within the β -sheets. Asparagine, on the other hand, has a side chain that may be too short to favor entropic freedom over the benefits of its side chain hydrogen bond stabilization. The side chain of this

residue may also lack the potentially beneficial hydrophobic length that the glutamine side chain possesses. Thus, A β_{16-22} peptides mutated with asparagine take on parallel β -sheet conformation no matter where the mutation is in the inner sequence in order to create Asn-Asn side chain hydrogen bonding and to preserve ring stacking. These results are consistent with statistical studies that show a propensity for asparagine to be included in parallel β -sheets, as mutations with this residue promote parallel β -sheets even in an amyloidogenic peptide known to form stable antiparallel β -sheets.

Future directions of this project may include the use of isotope-edited FTIR to determine if asparagine indeed forms hydrogen bonds across parallel strands. Slightly heavier ^{13}C in the carbonyl side chains of asparagine residues would create a distinguishing peak in the FTIR if asparagines were in close contact through hydrogen bonding. The same situation could be staged for glutamine side chains to determine their interaction behavior in the β -sheets. This technique of isotope labeling would also help us determine if the β -sheets were formed in-register, an important aspect of our theories that has been assumed up until this point. Additional computational simulations with larger peptide systems may also be able to further enhance the experimental data we collect about the peptide mutants. With new information gained about the effects small differences between amino acids like asparagine and glutamine have on the critical first steps of β -sheet formation in degenerative disorders, we hope to gain better insight on the fragile balances that help govern these complex diseases.

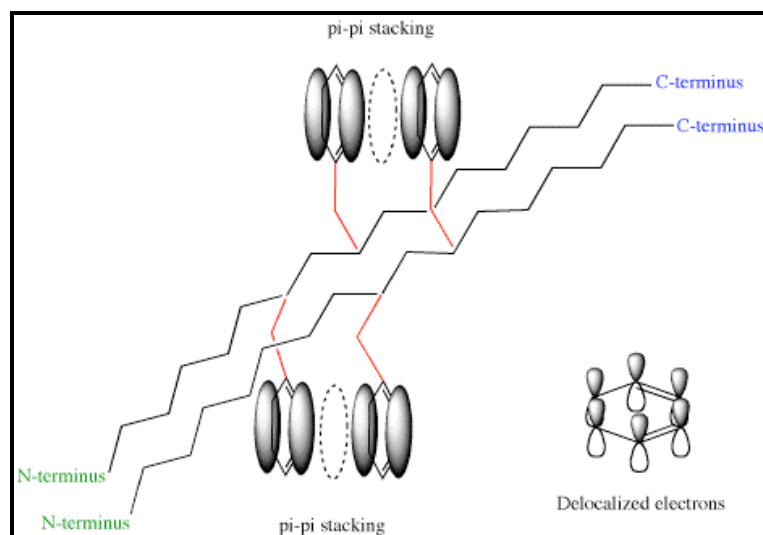


Figure 4.1 – Schematic of the positions and ring stacking behavior of phenylalanine residues at positions 19 and 20 if two $A\beta_{16-22}$ peptides were oriented in parallel β -sheets. The backbone of each strand is represented by a zigzag line. Dark rings around the aromatic rings in the phenylalanine side chains represent the electron delocalization caused by pi orbitals, shown explicitly on the right.

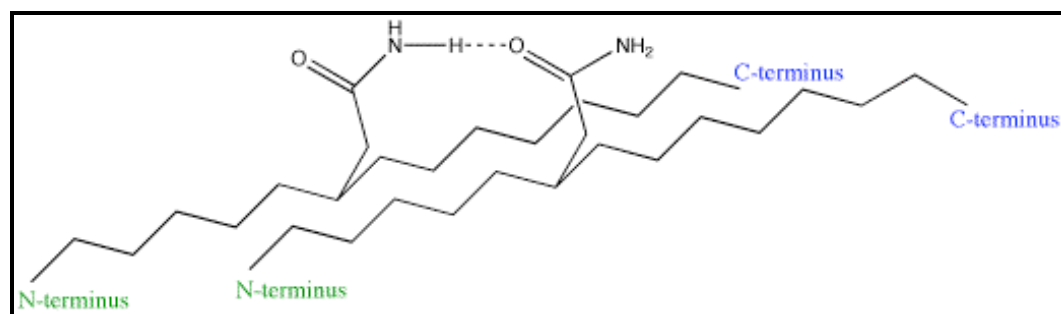


Figure 4.2 – Schematic of asparagine side chain hydrogen bonding in parallel β -sheets. The backbone of each strand is represented by a zigzag line and termini are positions are noted.

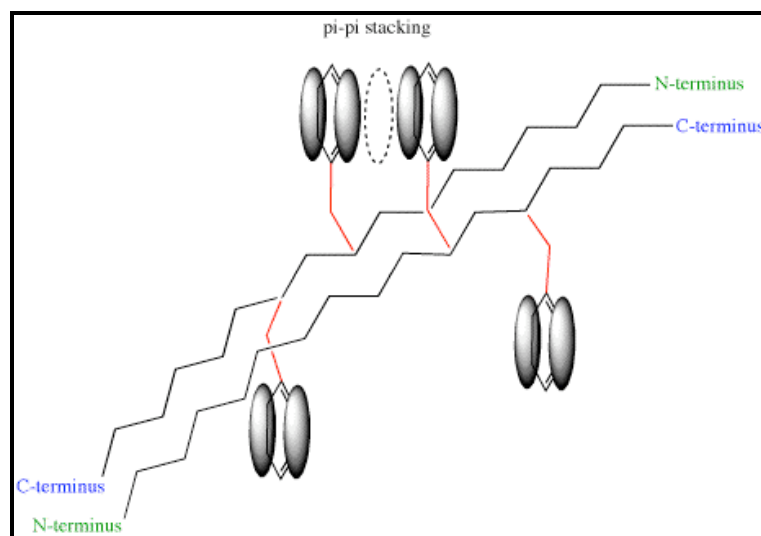


Figure 4.3 – Schematic of the positions and ring stacking behavior of phenylalanine residues at positions 19 and 20 in two $A\beta_{16-22}$ peptides if they were oriented in antiparallel β -sheets. The backbone of each strand is represented by a zigzag line. Dark rings around the aromatic rings in the phenylalanine side chains represent the electron delocalization caused by pi orbitals.

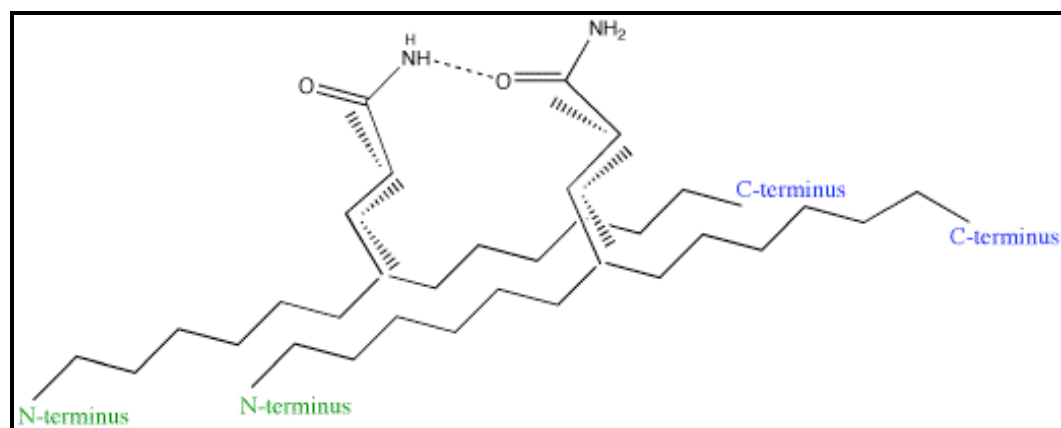


Figure 4.4 – Schematic of glutamine side chain hydrogen bonding in parallel β -sheets. The backbone of each strand is represented by a zigzag line and termini are positions are noted. The wedged lines along the side chain bonds depict entropic loss.

REFERENCES

- ¹ Nelson DL and Cox MM. Lehninger Principles of Biochemistry. 4th Ed. W.H. Freeman and Company. New York, NY (2005).
- ² Lesk, AM. Introduction to Protein Architecture. Oxford University Press. New York, NY (2001).
- ³ Baldwin RL and Rose GD. Is protein folding hierarchic? I. Local structure and peptide folding. *Trends Biochem Sci.* (1999) 24(1): 26-33.
- ⁴ Ramachandran GN and Sasiskharan. Conformation of Polypeptides and Proteins. *V. Adv. Protein Chem.* (1968) 23: 283-437.
- ⁵ Dobson CM. Protein folding and misfolding. *Nature.* (2003) 426: 884-890.
- ⁶ Dobson CM. The structural basis of protein folding and its link with human disease. *Phil. Trans. R. Soc. Lond.* (2001) 356: 133-145.
- ⁷ Finkelstein AV. Cunning simplicity of a hierarchical folding. *J Biomol Struct Dyn.* (2002) 20(3): 311-3.
- ⁸ Makin OS and Serpell LC. Structures for amyloid fibrils. *FEBS J.* (2005) 272(23): 5950-61.
- ⁹ Selkoe DJ. Folding proteins in fatal ways. Insight Review. *Nature* (2003) 426: 900-904.
- ¹⁰ Rochet, JC and Lansbury PT. Amyloid fibrillogenesis: themes and variations. *Curr. Opin. Struct. Biol.* (2000) 10: 60–68.
- ¹¹ López de la Paz M, Goldie K, Zurdo J, Lacroix E, Dobson CM, Hoenger A and Serrano L. De novo designed peptide-based amyloid fibrils. *Proc. Natl. Acad. Sci. USA* (2002) 99: 16052–16057.
- ¹² West MW, Wang W, Patterson J, Mancias JD, Beasley JR and Hecht MH. De novo amyloid proteins from designed combinatorial libraries. *Proc. Natl. Acad. Sci. USA* (1999) 96: 11211–11216.
- ¹³ Dyson HJ, Wright PE and Scheraga HA. The role of hydrophobic interactions in initiation and propagation of protein folding. *Proc. Natl. Acad. Sci. USA* (1996) 103(35): 13057-61.

- ¹⁴ López de la Paz M and Serrano L. Sequence determinants of amyloid fibril formation. *Proc Natl Acad Sci USA* (2004) 101: 87–92.
- ¹⁵ Fooks, HM, Martin, ACR, Woolfson DN, and Sessions RB. Amino acid pairing preferences in parallel β -sheets in proteins. *J. Mol. Biol.* (2006) 356: 32-34.
- ¹⁶ Haass C and Selkoe DJ. Soluble protein oligomers in neurodegeneration: lessons from the Alzheimer's amyloid-beta peptide. *Nature Reviews. Molecular Cell Biology* (2007) 8(2): 101-112.
- ¹⁰ Petty, SA, Adalsteinsson, T, and Decatur, SM. Correlations among morphology, beta-sheet stability, and molecular structure in prion peptide aggregates. *Biochemistry* (2005) 44(12): 4720-4726.
- ¹⁷ Antzutkin ON, Balbach JJ, Leapman RD, Rizzo NW, Reed J & Tycko R. Multiple quantum solid-state NMR indicates a parallel, not antiparallel, organization of beta-sheets in Alzheimer's beta-amyloid fibrils. *Proc Natl Acad Sci USA* 97: 13045–13050. (2000)
- ¹⁸ Balbach JJ, Petkova AT, Oyler NA, Antzutkin ON, Gordon DJ, Meredith SC & Tycko R. Supramolecular structure in full-length Alzheimer's beta-amyloid fibrils: evidence for a parallel beta-sheet organization from solid-state nuclear magnetic resonance. *Biophys J* (2002) 83: 1205–1216.
- ¹⁹ Balbach, JJ, et al. Amyloid fibril formation by A-Beta (16-22), a seven-residue fragment of the Alzheimer's beta-amyloid peptide, and structural characterization by solid state NMR. *Biochemistry* (2000) 39(45): 13748-13759.
- ²⁰ Petty, SA and Decatur, SM. Experimental evidence for the reorganization of β -strands of the A β ₁₆₋₂₂ peptide. *J. Am. Chem. Soc.* (2005) 127(39): 13488–13489.
- ²¹ McQuarrie, DA and Simon, JD. Physical Chemistry: A Molecular Approach. University Science Books, Sausalito, California. 1997.
- ²² Barth A and Zscherp C. What vibrations tell us about proteins. *Quarterly Reviews of Biophysics* (2002) 35(4): 369-430.
- ²³ Surewicz WK, Mantsch HH, and Chapman D. Determination of protein secondary structure by Fourier transform infrared spectroscopy: a critical assessment. *Biochemistry* (1993) 32, 389-394.

- ²⁴ Brooks CL, Karplus MK, and Pettitt BM. Proteins: A Theoretical Perspective of Dynamics, Structure, and Thermodynamics. John Wiley and Sons, Toronto. 1988.
- ²⁵ “Amino Acid.” The Molecular Workbench. 2006. The Concord Consortium. Accessed March 2007. <http://workbench.concord.org/web_content/unitV/images/amino_acid1.gif>
- ²⁶ “Amino Acid Table”. Bioweb. 2002. The Board of Regents of the University of Wisconsin System. Accessed April 2007. <http://bioweb.uwlax.edu/GenWeb/Molecular/Bioinformatics/Unit_4/Lab_4-1/amino.gif>
- ²⁷ “Section 3.5: Peptide Bonds.” BIOC 380 Fall 2006 Lecture Notes. 2006. University of Montana. Accessed March 2007. <<http://dbs.umt.edu/courses/fall2006/bioc380/lectures/008/lecture.html>>
- ²⁸ “Planarity of the Peptide Bonds.” BIOC 380 Fall 2006 Lecture Notes. 2006. University of Montana. Accessed March 2007. <<http://dbs.umt.edu/courses/fall2006/bioc380/lectures/010/lecture.html>>
- ²⁹ “Parameters of Protein Conformation.” BIOC 380 Fall 2006 Lecture Notes. 2006. University of Montana. Accessed March 2007. <<http://dbs.umt.edu/courses/fall2006/bioc380/lectures/010/lecture.html>>
- ³⁰ “Ramachandran Diagrams.” BIOC 380 Fall 2006 Lecture Notes. 2006. University of Montana. Accessed March 2007. <<http://dbs.umt.edu/courses/fall2006/bioc380/lectures/010/lecture.html>>
- ³¹ “Geometry of β -Sheets.” BIOC 380 Fall 2006 Lecture Notes. 2006. University of Montana. March 2007. <<http://dbs.umt.edu/courses/fall2006/bioc380/lectures/011/lecture.html>>
- ³² Glabe, CG. Common mechanisms of amyloid oligomer pathogenesis in degenerative disease. *Neurobiology of Aging* (2006) 27(4): 570-5.
- ³³ “Translation Genetics.” Biocrawler. 1996. Accessed April 2007. <<http://www.biocrawler.com/w/images/thumb/c/cf/300px-Translation-genetics.png>>
- ³⁴ Horton et al. Principles of Biochemistry. 4th ed. Prentice Hall, NY. (2005).

- ³⁵ “How the Brain and Nerve Cells Change During Alzheimer’s Disease.” American Health Assistance Foundation. 2007. American Health Assistance Foundation. March 2007. <http://www.ahaf.org/alzdis/about/Brain_Neurons_AD_Normal.htm>
- ³⁶ Luhrs T, Ritter C, Adrian M, Riek-Loher D, Bohrmann B, Dobeli H, Schubert D, and Riek R. 3D structure of Alzheimer's amyloid- β (1-42) fibrils. *Proc .Natl. Acad. Sci. USA* (2005) 102: 17342-17347.
- ³⁷ Cole EB. Structure and aggregation of the nucleating core of islet amyloid polypeptide (IAPP). 2006. Bachelor of Arts Thesis, Mount Holyoke College.
- ³⁸ MacKerrell AD, Banavali N and Foloppe N. Development and current status of the CHARMM force field for nucleic acids. *Biopolymers (Nucleic Acid Sci)* (2001) 56: 257-265.
- ³⁹ “HPLC System Diagram.” HPLC Primer. 2007. Waters Corporation. Accessed April 2007. <<http://www.waters.com/WatersDivision/ContentD.asp?watersit=JDRS-6UXGYA>>
- ⁴⁰ “Energy Landscape Images.” Dr. Mario Pavone. Protein Structure Prediction. 2007. The University of Catania. Accessed April 2007. <<http://www.dmi.unict.it/~mpavone/landscape.html>>
- ⁴¹ Zhou R. Free energy landscape of protein folding in water: explicit vs. implicit solvent. *Proteins: Structure, Function and Genetics* (2003) 53(2): 148-161.